

Pore-water chemistry of sediment cores off Mahanadi Basin, Bay of Bengal: Possible link to deep seated methane hydrate deposit

A. Mazumdar^{1*}, A. Peketi², H.M Joao³, P. Dewangan⁴, T. Ramprasad⁵

^{1,3,4,5}National Institute of Oceanography, Dona Paula,
Goa-403 004, India.

²Physical Research Laboratory, Ahmedabad, Gujarat-380 009, India

**for correspondence: maninda@nio.org*

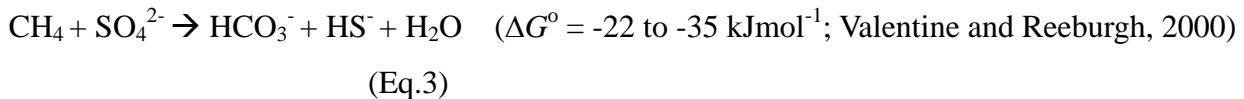
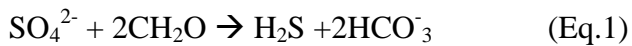
Abstract

Organoclastic degradation and anaerobic oxidation of methane (AOM) are known to influence sulfate, methane and bicarbonate concentrations of sediment pore-waters. In this work we have analysed the pore-fluid composition of three piston cores (36-39 m long) collected from water depths ranging from 1429 to 1691 m. We attribute the observed linear sulfate concentration profiles and $(\Delta\text{Ca}+\Delta\text{Alk})/\Delta\text{SO}_4^{2-}$ ratios dominantly to anaerobic oxidation of methane (AOM) induced sulfate consumption. The gas rich layers just below the base of hydrate stability zone (BGHSZ) is the possible source of the enhanced diffusive flux of biogenic methane ($\delta^{13}\text{C}_{\text{CH}_4}$ ranging from -99.7 to -106.3 ‰ VPDB). Occurrences of disseminated gas hydrate in the Mahanadi basin within the hydrate stability zone (210 to 220 m thick) supports the link between linear sulfate profile, high rate of AOM and hydrate occurrence.

Keywords: AOM, Mahanadi basin, sulfate reduction, sulfate profile, SMTZ

1. Introduction

The composition of the fluid and some solid phases in the marine sediments are controlled by various geological (depositional and structural) and biogeochemical processes which are closely interlinked (Berner, 1980; Canfield et al., 2005a; Coffin et al., 2007). Abundance of labile organic matter in the sediments drives the biogeochemical cycles. The burial flux of labile organic matter fueling the bacterially mediated reactions depends on the oxygen exposure time, which in turn is controlled by sedimentation rate, bioturbation, organic flux and oxygen availability at the sediment water interface (Westrich and Berner, 1984; Hedges and Keil, 1995; Hartnett et al., 1998; Gélinas et al., 2001; Rontani et al., 2012; Koho et al., 2013). Evolution of sediment pore-fluid composition during burial is governed by bacterially driven sub aerobic/ anaerobic remineralization processes like reduction of nitrate, iron, manganese, sulfate, CO₂ and oxidation of sulfide and methane (Schulz and Zabel, 2000). Bacterial sulfate reduction (Eqs.1-2) accounts for the bulk of the organic matter remineralization in marine sediments through anaerobic pathways (Jørgensen, 1977; Sorensen et al., 1981; Jørgensen, 1982; Canfield, 1989; Kristensen, 2000).



Free energy yield (ΔG^0) during sulfate reduction depends on the electron donors (substrate). Fermentation products like acetate, lactate, formate and H₂ are the common substrates in organic rich sediments. Brüchert (2004) compiled the ΔG^0 values (-45 to -340 kJmol⁻¹ SO₄²⁻) for a wide range of substrates. In dissimilatory sulfate (SO₄²⁻) reduction (Harrison and Thode, 1958; Canfield, 2001; Megonigal et al., 2003; Canfield et al., 2005a) bacteria employ a respiratory mechanism with sulfate as the terminal electron acceptor giving rise to sulfide as the major metabolic end-product. It involves oxidative phosphorylation through an electron-transfer pathway (Rabus et al., 2007; Pereira et al., 2011). A range of proteins viz., a sulfate transporter, Sat, a pyrophosphatase, AprAB, DsrAB, DsrC, DsrMK, and Fd involved in the metabolic pathway leading to sulfate reduction are reported by Pereira et al. (2011). Sulfate reduction results in the breakdown of S-O bonds of dissolved sulfate and subsequent

production of H₂S. During this transition, the valence state of sulfur changes from +6 to -2, i.e., a net transfer of 8 electrons via enzymatic pathways (Canfield, 2001). Sulfate reducing bacteria are most active close to the sediment water interface owing to high labile organic load and sulfate flux at the interface (Kasten and Jørgensen, 2000; Megonigal et al., 2003, Wall et al., 2008). Rate of sulfate reduction in marine sediments depends mainly on the availability of labile organic compounds which serve as substrate for sulfate reducing bacteria (SRB) (Madigan et al., 2000), temperature (Westrich and Berner, 1988; Canfield et al., 2006), bacterial species (Brüchert, 2004), sedimentation rate (Goldhaber and Kaplan, 1975; Berner, 1978; Canfield 1989; Claypool, 2004), sulfate concentrations (Canfield, 2005b); energy availability (Jin and Bethke, 2009) and possibly bioturbation.

Other than organo-clastic sulfate reduction, bacterially mediated anaerobic oxidation of methane (AOM: Eq. 3), profoundly contribute towards sulfate consumption (Borowski et al., 1996, 1999; Niewohner et al., 1998). AOM is performed by a syntrophic consortium of methanotrophic archaea and sulfate-reducing bacteria (Boetius et al., 2000; Orphan et al., 2001; Reeburgh, 2007; Knittel and Boetius, 2009; Milucka et al., 2012). Environmental genomic and proteomic studies (Krüger et al., 2003; Hallam et al., 2004; Scheller et al., 2010) suggest a strong phylogenetic link between the methanogens and methanotrophic archaea (ANME I and II). AOM reduces the release of methane into the atmosphere from ocean sediments, which would otherwise cause a major increase in green house gas concentrations (Lashof and Ahuja, 1990). AOM consumes >90% of the total methane produced (85-300 Tg CH₄ year⁻¹) annually in the oceanic sediments (Hinrichs and Boetius, 2002; Reeburgh, 2007).

The zone within anoxic sediment column where pore-water sulfate and methane concentration profiles intersect and may reach non-detectable levels is known as the sulfate-methane transition zone (SMTZ). The depth of SMTZ as well as the concentration gradients are markedly influenced by the methane flux (Borowski et al., 2000). High methane flux in the sediment may also lead to enhanced methane saturation promoting gas hydrate formation under suitable temperature-pressure conditions (Kvenvolden, 1993; Sloan, 1998). Methane hydrate is an ice like crystalline solid in which methane and other lighter hydrocarbon gases are trapped inside a cage like structure of water molecules (Sloan, 1998). Attempts have been made earlier to use methane flux, nature of sulfate profile and the depth of the SMTZ as tools for gas hydrate exploration (Borowski et al., 1996; 1999; Bhatnagar et al., 2008; Mazumdar et al., 2012).

Seismic data as well as drilling and logging activities onboard JOIDES *Resolution* in the Indian continental margins, under the aegis of Indian national gas hydrate program (NGHP) show the existence of disseminated gas hydrate in the Mahanadi basin (Collett et al., 2008). Our coring sites MD161-1-19 and MD-161-25 are close to the NGHP expedition-01 drilling/coring sites NGHP-01-19 and NGHP-01-18 respectively (Fig. 1). The other coring site MD161-27 is ~25 km from NGHP-01-08 site (Fig. 1). Pore-water chlorinity measurements in cores NGHP-01-18 and NGHP-01-19 show marked freshening within 140-160 and 120-190 mbsf respectively, suggesting thawing of methane hydrate during core recovery which releases fresh water into the sediment pores thereby lowering the chloride concentrations. The Infrared (IR) anomaly of the sediment cores at these sites show cold spots attributed to the thawing of hydrates. Geophysical logging data and x-ray imaging of pressure cores at the Site NGHP-01-19 further support the occurrences of gas hydrates as disseminated thin layers. In the present work we have attempted to explain the origin of sulfate profiles, genesis/ source of methane and the possible link between methane hydrate and observed biogeochemical profiles.

2. Geological framework

Mahanadi is one of the major rivers in India, flowing eastwards and draining into the Bay of Bengal. The detrital load to the Mahanadi offshore is brought by the Mahandi River system. Mahanadi offshore is a well known petroliferous basin located along the East coast of India (Singh, 2008). Mahanadi Basin extends from Jagannathpur in the north to Chilka lake in the south and further extending to the offshore in the Bay of Bengal (Fig. 1). It is a passive pericratonic basin covering an area of 2,60,000 km² with water depth exceeding 3000 m (including deep offshore) (Singh, 2008). The shelf break occurs approximately along the 150 m isobath. Mahanadi offshore area represents a pull apart type of basin which generally parallels the coast with sedimentary section showing rapid seaward thickening (Jagannathan et al., 1983). The basin originated during the break-up of Gondwanaland in Late Jurassic time. Mahanadi basin is believed to have been formed at one of the three fossil triple junctions identified along the east coast of India (Burke and Dewey, 1973). The basement configuration inferred from the bathymetry, magnetic and gravity modelling resembles a series of coast-parallel structural highs and depressions (Subrahmanyam et al., 2008). Tectonically, the basin extends from Damra-Wheeler lineament in the north to 85° E ridge in the south. In the west, the basin continues with Hasdo-Mahanadi Gondwana graben (Mohapatra, 2006). The basement is covered by volcanic and sedimentary sequences

ranging in age from Cretaceous to Holocene. The Lower Cretaceous volcanic and intertrappeans are successively overlain by Paleocene sand/silt/clay, Eocene carbonates, Lower to Middle Miocene clays/silt/minor limestone and Pliocene to younger sands/silts/clays (Jagannathan et al., 1983; Singh, 2008).

3. Methodology

3.1 Geophysical/ geological

Sub-Bottom Profiler (SBP) data was collected using a Seafalcon 11 echosounder onboard *Marion Dufresne*. This system produces high-resolution, zero-offset acoustic sections of the sub-surface as a function of the geographical position of the ship. The central frequency used in this system was 3.75 KHz.

Porosity of the sediment was calculated from the difference in wet and dry weights of sediments. Dry weight of the sediments was measured after drying it at 105°C.

3.2 Geochemical

A giant Calypso piston corer was used on board ORV *Marion Dufresne* (MD-161) for the retrieval of sediment cores off Mahanadi Basin over water depth ranging from 1429 to 1691 m. Sampling locations are shown in Figure-1. PVC liners of 10 cm inner diameter were used for core collection. Sub-sampling was carried out by cutting out 10 cm thick sediment slabs along with the liner at 1 or 1.5 meter intervals within one and a half hour of core retrieval. Sub-sampling for gas (absorbed and dissolved) was carried out using a 10 ml cut-syringe from the core of the sediment slabs to minimize atmospheric contamination. Sediment was stored in 28 ml glass vials with 5 ml of 0.5 M sodium azide (bacteriacide) and crimped immediately following nitrogen flushing. Sediment was homogenized using a vortex shaker and stored at 2°C until concentrations of hydrocarbon (CH₄, C₂H₆ and C₃H₈) gases in the head space were measured using a Varian Gas chromatograph (CP 3380). After sub-sampling for gas, sediment slabs were immediately transferred into thick plastic bags, filled with high purity nitrogen and heat sealed to avoid atmospheric oxygen contamination which can oxidize hydrogen sulfide or iron monosulfide. Pore-water was extracted from the sediments using a Manheim type hydraulic press following standard ODP protocol (Sayles et al.,1973; Gieskes, 1974). Pore-waters were

collected in 20 ml plastic syringes with Luer lock. They were filtered through a 0.2 micron Whatman syringe filter, stored in crimp vials under nitrogen head and preserved at 2°C. Total alkalinity (Gieskes and Peretsman, 1986) was measured on-board following Gran titration method using a Metrohm Autotitrator (Titrino 799 GPT). Sulfate concentrations were measured using a Dionex-600 ion chromatograph (Gieskes et al., 1991). Prior to sample injection, 1 ml of pore-water sample was diluted to 50 ml or 100 ml and passed through silver cartridge to remove chloride ion. An IonPac AS9-HC column was used for ion separation and ASRS Ultra-II (2 mm) was used as anion self-regenerating suppressor. Calibration curve was prepared using standard IC sulfate solution from Dionex. The calibration line was cross checked with Dionex anion mixed standard. A precision of 0.5 to 1% is reported here. Measurement of hydrogen sulfide concentrations was attempted spectrophotometrically using H₂S-NN dimethyl-p-phenylenediaminesulfate complexation method following Cline (1969). Ammonia in pore-waters was measured spectrophotometrically following the indophenol blue method (Koroleff, 1976). A Chemito spectrophotometer (Spectroscan UV 2700) was used for this purpose.

Calcium concentration in the pore-waters was measured using an ICP-AES (Model:Thermo Electron IRIS INTREPID II XSP DUO) following suitable dilution. A precision of 1% is reported for calcium and magnesium concentration measurement.

Carbon stable isotope ratios of head space gases were measured using a Thermo Delta V continuous flow isotope ratio mass spectrometer attached to a gas chromatograph (Thermo trace GC). The external precision is typically 0.07–0.09 ‰ VPDB for $\delta^{13}\text{C}$ based on long term measurement of cellulose standard IAEA-C3. Total carbon (TC) content of sediments was measured by elemental analyzer (Thermo EA1112). The carbon content was cross checked with MAG-1 (USGS) standard. Total inorganic carbon (TIC) content was measured by UIC carbon coulometer (CM 5130). Ultrapure CaCO₃ (Sigma-Aldrich) was used as standard for TIC measurement. Precision for TC and TIC measurements are 1 and 1.4% respectively. Total organic carbon (TOC) was calculated by subtracting TIC from TC.

AMS ¹⁴C dates were generated at the National Ocean Sciences AMS (NOSAMS) facility, Woods Hole Oceanographic Institution, USA. Dates were determined on planktonic foraminifera species *Globigerina ruber* and *Globigerina sacculifer*. Carbon dioxide generated from these foraminifera shells was reacted with catalyst to form graphite which was pressed into targets and analyzed on the

accelerator along with standards and process blanks. Two primary standards used during ^{14}C measurements are NBS Oxalic Acid I (NIST-SRM-4990) and Oxalic Acid II (NIST-SRM-4990C).

3.3 Computational

Diffusive sulfate (J_{SO_4}) and methane fluxes (J_{CH_4}) were calculated from the concentration profiles using Fick's first law (Eq-4) assuming steady state conditions (Berner, 1980; Canfield, 1989, 1991),

$$J_{\text{SO}_4} = \phi D_s (dC/dX) \quad (\text{Eq.4})$$

where J , C and ϕ represent the depth-integrated sulfate reduction/ methane oxidation rate ($\text{mmol m}^{-2} \text{yr}^{-1}$), sulfate/ methane concentration (mM) in the pore-water and average sediment porosity respectively. dC/dX is the sulfate/ methane concentration gradient and D_s ($\text{cm}^2 \text{sec}^{-1}$) is the molecular diffusivity corrected for tortuosity. D_s is calculated by the formula

$$D_s = D_o/[1+n(1-\phi)] \quad (\text{Eq.5})$$

where $n = 3$ for clays and silt (Iversen and Jørgensen, 1993). D_o = sulfate/ methane diffusivity in the absence of particles. Since D_o varies with temperature (water depth), we have calculated D_o at different temperatures using an empirical relation based on data set from Li and Gregory, (1974). In this study, advective pore-water transport (eg. Bioirrigation) or reoxidation of sulfide within the sediment have been neglected. Assessing the error in calculation due to this limitation is beyond the scope of the present work. Grain size data for flux calculation are taken are from Mazumdar et al., (*in prep.*).

4. Results

4.1 Geological

The multibeam bathymetry data (Fig. 1) show numerous coast-perpendicular canyons originating at shelf break within the water depth of 600-800 m and terminating at continental rise between 1800 and 2000 m. The regional sub-bottom profiler data (Fig. 2) shows steep canyons (~ 150 m deep). Draped, continuous, well-laminated sediments are observed in the SBP data covering the valley floor. No evidence of slumping and sliding events is observed at all the coring sites (MD161/19, 25 and 27). In

addition, no seismic signatures of shallow gas charged sediments like acoustic chimneys, acoustic turbidity, etc are observed in the vicinity of coring sites.

The average porosity in the studied cores range from 67.5 to 72 %.

4.2 Geochemical

4.2.1 Radiocarbon ages

Age depth curve for MD161-19 is given in Figure 4. Radiocarbon ages are converted to mean calendar ages following the calibration curve of Fairbanks et al. (2005) and the calibration software (<http://radiocarbon.ldeo.columbia.edu/research/radcarbcal.htm>). The top 1 m show high sedimentation rate of 241 cm/ky. Holocene sedimentation rates (SR) at this site range from 35 to 241 cm/ky. The pre-Holocene sediment package shows more or less uniform sedimentation rate of ~8 cm/ky. The Toba ash bed layer dated ~74 ky BP (Ninkovitch, 1979; Acharyya and Basu, 1993), recorded at a depth of 9.05 mbsf in MD161-19 (Kocherla et al., *in prep.*) fits closely with the C-14 based age-depth model curve (Fig. 4).

4.2.2 Total Organic Carbon content and Ammonium profile

Total organic carbon (TOC: Fig. 5) content ranges from 0.6 to 2 wt% (Avg.: 1.1 ± 0.2 wt%). Relative to MD161-25 and 27, higher TOC content is recorded in MD161-19. At all the sites, ammonium concentrations (Fig. 6) in the pore-waters increase with depth below the sediment-water interface. At the core top NH_4^+ concentrations range from 35 to 47 μM . The maximum NH_4^+ concentrations with depth range from 969 to 1490 μM . A sharp increase in concentration is noted in MD161-25 at a depth of 29.55 mbsf (Fig. 6).

4.2.3 Sulfate-methane-alkalinity and Calcium concentration profiles

Sulfate-methane-alkalinity profiles for the three coring sites (MD161-19, 25 and 27) are plotted in Figure 7 (A-C). The sulfate concentration profiles are of quasi-linear type. The sulfate concentration gradients for MD161-19, 25 and 27 are 1.61, 1.73 and 1.62 mM/m, respectively (Fig. 7 A to C). The J_{SO_4} for MD161-19, 25 and 27 are 10.2, 12.8 and 11.3 $\text{mmol m}^{-2}\text{y}^{-1}$ respectively. The thickness of sulfate methane transition zone (SMTZ) ranges from 3 to 4.5 m. Methane concentrations increase

sharply below the SMTZ and show highly variable gradients. We have not detected hydrogen sulfide in any of the cores.

J_{CH_4} values for MD161-19, 25 and 27 are 13.5, 2.1 and 3.9 $mmolm^{-2}y^{-1}$ respectively. Total alkalinity (TA) profiles (Fig. 7) show steady increase from core top (4-4.7 mM) to the SMTZ (23.3 to 27.2 mM) followed by a relatively gentler drop (17.5 to 20.2 mM) at the bottom of the cores. In case of MD161-27, TA remains steady (18.8 to 20.2 mM) within the depth range of 25 to 35.5 mbsf. Pore-water calcium concentrations decrease with depth below sediment water interface at all the three sites (Fig. 8). The core top Ca concentrations range from 12.4 to 15.8 mM, whereas, at deeper layers the Ca concentrations range from 2.7 to 5.7 mM. Cross plot of $(\Delta Ca + \Delta Alk)$ vs. ΔSO_4^{2-} (Fig. 9) show clustering of data points around the 1:1 and 2:1 lines. The Mg concentration has not been used in the above plot due to large fluctuations observed in the depth profile Mg (Table-1).

4.2.4 Methane and CO₂ carbon stable isotope profiles

Carbon stable isotope ratios of CH₄ and CO₂ gases in the headspaces are plotted in Figure 10(A-C). Close to the SMTZ, $\delta^{13}C_{CH_4}$ reaches minima which range from -99.7 to -106.3 ‰ VPDB. The $\delta^{13}C_{CH_4}$ increases gently down depth below SMTZ and shows a parallel trend with $\delta^{13}C_{CO_2}$. Carbon isotope ratios of CO₂ show enrichment with depth below SMTZ. Low $\delta^{13}C_{CO_2}$ values (-24.9 to -30.8 ‰ VPDB) are recorded close to the SMTZ. $\Delta\delta_{CO_2-CH_4}$ (ϵ) below SMTZ ranges from 70 to 80 ‰ VPDB (Avg.: 74.9 ± 3.8 ‰ VPDB) and shows low variability at individual sites. $\delta^{13}C_{CH_4}$ increases sharply above SMTZ and approaches $\delta^{13}C_{CO_2}$ values. The sharp increase in $\delta^{13}C_{CH_4}$ is also shown in Figure-11, which shows the variations in $\delta^{13}C_{CH_4}$ with C1/(C2+C3) ratios. Below SMTZ, C1/(C2+C3) ratio range from 772 to 5128. C1, C2 and C3 represent concentrations of methane (CH₄), ethane (C₂H₆) and propane (C₃H₈) respectively.

5. Discussion

5.1 Evidences of subsurface gas hydrate in Mahanadi basin

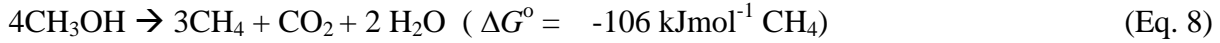
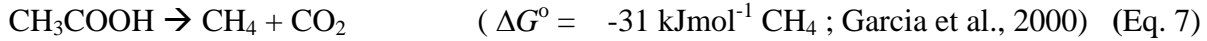
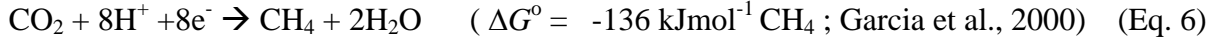
The regional presence of gas hydrates is inferred from the presence of well developed bottom simulating reflector (BSR) in the seismic profile (Fig. 3: reproduced from Collett, et al., 2008). The BSR is believed to appear due to the acoustic impedance contrast between the overlying gas hydrate

deposit and the underlying free gas layer. BSR may also form due to the presence of small amount of free gas below the hydrate stability zone with negligible presence of gas hydrate (Hyndman and Spence, 1992). The occurrence of high amplitude reflectors below the BSR suggests the presence of gas charged sediments. Analysis of resistivity log data acquired on board *JOIDES resolution* during Indian National Gas Hydrate Program (NGHP-01: Collett et al., 2008) at Site NGHP-01-19 shows ~15 % gas hydrate saturation in the hydrate stability zone (220 mbsf). Other indirect evidences of hydrates include pore-water freshening, high methane concentrations in excess of saturation in the pressure cores and IR anomalies suggesting the presence of disseminated methane hydrate within the silty-clay matrix. Several high angle faults disrupting the overburden sediment are observed clearly in the seismic profiles. In addition, the seismic data shows structures akin to cut-and-fill deposits which may act as the loci for hydrate crystallisation if they are filled with coarse grained sediments. Estimated seabed temperature at this site is about 4.8 °C and thermal gradient is 53 °C/km (Collett et al., 2008).

The laminated nature (SBP data: Fig. 2) of the sediments and the absence of slumping/sliding like features in the vicinity of coring sites suggest continuous sedimentation at the coring sites. The continuity in sedimentation is further supported by radiocarbon based age-depth model at MD161-19 (Fig. 4).

5.2 Methanogenesis and Methanotrophy

Methanogenic archaea produce methane under strictly anaerobic conditions where CO₂, a by-product of organic fermentation, plays the role of electron acceptor leading to the methane production (Martens and Berner, 1974; Jarrel, 1985; Canfield et al., 2005b, Walker et al., 2012). Methanogens can produce methane only in anoxic sediments owing to instability of their F420-hydrogenase enzyme complex in the presence of O₂, nitrate or nitrite (Scönheit et al., 1981). The dominant methanogenic pathway in marine sediment is carbon dioxide (CO₂) reduction by hydrogen (H₂) (hydrogenotrophic pathway: Eq. 6). Other known pathways include methanogenesis from acetate cleavage (acetoclastic pathway, Eq. 7) and methanogenesis from methylated compounds such as methanol and methylated amines (methylotrophic pathway, Eq. 8) (Whiticar and Faber, 1986; Alperin et al., 1992; Whiticar, 1999; Conrad, 2005; Galimov, 2006; Reeburgh, 2007).



Above SMTZ, sulfate reducers out compete methanogens for competitive substrates (eg. acetate and H₂) in sulfate rich pore-waters. Whereas, below the zone of sulfate reduction, hydrogenotrophy (CO₂ reduction) is the dominant methanogenic pathway since other methanogenic substrate, like acetate, are depleted due to organo-clastic sulfate reduction (Whiticar and Faber, 1986; Whiticar, 1999; Conrad, 2005; Galimov, 2006). Methane concentrations increase sharply below the SMTZ (Fig. 7). However, down depth, the profiles show significant fluctuations possibly owing to heterogeneous distribution of gas pockets or degassing during core recovery and onboard sub-sampling (Dickens et al., 1997; Paull and Ussler III, 2001). The methane concentrations and fluxes reported in the present work are possibly much lower than the in situ concentrations. Fluctuations in the methane concentration profiles have earlier been reported from Mahanadi basin by Collett et al. (2008). Highly depleted carbon isotopic compositions of methane below the SMTZ (-99.7 to -106.3 ‰VPDB), high C₁/(C₂+C₃) hydrocarbon ratios (772 to 5128) and Δδ_{CO₂-CH₄} ranging from 70 to 80 ‰ VPDP indicate the microbial origin of methane in Mahanadi basin via CO₂ reduction pathway. Other factors which may influence δ¹³C_{CH₄} include methanogenic precursor, fractionation factor and temperature etc. (Alperin et al., 1992; Whiticar, 1999). The possible contribution of acetate fermentation in methanogenesis is difficult to assess in the absence of δD_{CH₄}, δ¹³C_{acetate} and acetate concentration measurements (Conrad, 2005). The down depth enrichment in the carbon isotope ratio of methane may be attributed to the continued preferential removal of the isotopically lighter molecules from the carbon pool (CO₂) during methanogenesis resulting in a progressive shift in the residual substrate towards enriched carbon isotope ratios following Rayleigh fractionation (Whiticar, 1999). The down depth enrichment in methane concentrations eventually leads to methane hydrate crystallization within the hydrate stability zone (Kvenvolden, 1993; Kvenvolden and Loreson, 2001; Milkov et al., 2005). Below the BGHSZ, the degassing of crystalline gas hydrate owing to continued sedimentation and burial, results in buildup of free gas under the hydrate layer. The occurrence of hydrate and free gas results in the appearance of well-defined BSR in the seismic data of Mahanadi. The nature of methane concentration profile close

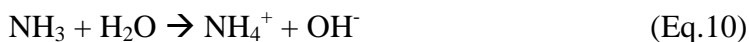
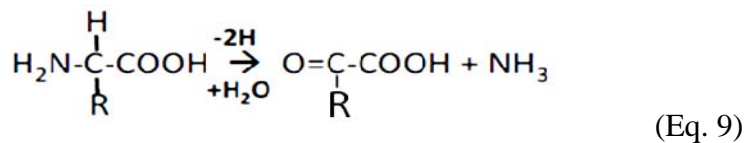
to SMTZ is a result of methane consumption via AOM typically represented by Eq. 3. The drastically low values of C1/(C2+C3) hydrocarbon ratios (Table-1) at SMTZ suggest preferential bacterial consumption of methane at the SMTZ due to AOM. The $\delta^{13}\text{C}_{\text{CH}_4}$ shows exponential increase with decrease in C1/(C2+C3) hydrocarbon ratios (Fig. 11). As CH_4 is continually removed, the molecular fractionation results in relative enrichment of the residual hydrocarbon gas in the higher homologues (ethane, butane, propane). The bacterial uptake of CH_4 is associated with a kinetic isotopic enrichment (KIE) that enriches the residual CH_4 in the heavier isotope (Alperin et al., 1988; Whiticar, 1999, Whiticar, 2002). The KIE of ^{13}C in the residual methane may be attributed to preferential breakdown of ^{12}C -H bond (Hofstetter et al., 2008). The headspace $\delta^{13}\text{C}_{\text{CO}_2}$ shows a shift towards ^{13}C depletion (-24.9 to -30.8 ‰ VPDB) close to SMTZ suggesting contribution of CO_2 from methane oxidation. Ussler III and Paull, (2008) also recorded depleted carbon isotope ratios of headspace CO_2 close to SMTZ from the northern Gulf of Mexico. Carbon isotope separation ($\Delta\delta_{\text{CO}_2\text{-CH}_4}$) between residual methane and CO_2 decreases upwards in the cores owing to decrease in CO_2 contribution from methane oxidation and increasing contribution of organo-clastics derived CO_2 which approaches $\delta^{13}\text{C}_{\text{TOC}}$. The $\delta^{13}\text{C}_{\text{TOC}}$ of Mahanadi basin ranges from -16.9 to -21.6 ‰ VPDB (Mazumdar et al., unpublished data). Towards the core top most enriched carbon isotope ratios are commonly recorded for CO_2 due to contribution from sea water DIC.

5.3 Total alkalinity and Ammonium trends

The total alkalinity (TA) values increase steadily down depth and reach maximum close to the SMTZ (Fig. 7). Below SMTZ, TA values drop with depth and show slight variation in the profiles. The slight parabolic character of the TA profiles across the SMTZ associated with the quasi-linear sulfate concentration trends are typical of AOM (Schmidt et al., 2005; Kastner et al., 2008; Ussler III and Paull, 2008; Mazumdar et al., 2012). Vertical diffusion of bicarbonate ions produced via focused sulfate reduction at the SMTZ is apparently responsible for the variable degree of parabolic character of the TA profiles (Ussler III and Paull, 2008). The relative contribution of AOM and organoclastic degradation towards alkalinity may be evaluated through the $(\Delta\text{Ca}+\Delta\text{Alk})/\Delta\text{SO}_4^{2-}$ ratios of pore-waters (Solomon et al., 2008; Chen et al., 2010; Burdige and Komada 2011; Malinverno and Pohlman, 2011). Sulfate reduction solely via organoclastic degradation produces 2 mol of HCO_3^- per mol of SO_4^{2-} reduced (Eq. 1), while AOM produces 1 mol of HCO_3^- per mol of sulfate reduced (Eq. 3). In the present

study, data points in ($\Delta\text{Ca}+\Delta\text{Alk}$) vs ΔSO_4^{2-} cross plot values of several pore-water samples fall on or close to the 1:1 line, where as few data points fall on the 1:2 line (Fig. 9). The clustering of the data points around the 1:1 line suggest a dominant contribution of pore-water bicarbonate via AOM pathway. However, further confirmation of influence of AOM relative to organoclastic degradation on sulfate reduction is possible through $\delta^{13}\text{C}_{\text{DIC}}$ values of pore-water (Solomon et al., 2008; Chen et al., 2010). Additional factors like silicate weathering (Wallmann et al., 2008) and/or degassing of CO_2 from the sediments during core recovery and sub-sampling (Paull and Ussler III, 2001) may also influence the pore-water alkalinity profiles.

Ammonium (NH_4^+) in marine sediments is produced via anaerobic bacterial decomposition of nitrogen bearing organic compounds (Heinrich and Reeburgh, 1987) utilizing anaerobic oxidants. Down depth build up of NH_4^+ in marine sediments (Fig. 6) is attributed to deamination pathway (Eqs. 9-10) which involves break down of amino acids and the removal of an amine group from the molecule catalyzed by enzyme called deaminases. Deamination of the amino acids derived from algal and other proteins will produce both organic acids and ammonium (Kuznetsov, 1975). Several different deamination pathways like hydrolytic deamination of amino acids and oligopeptides, degradation of nucleotides, and metabolism of methylamines by methanogens are known to operate in the marine sediments leading to NH_4^+ build up in pore-waters (Jacobsen et al., 1987).



Although NH_4^+ production and sulfate reduction have been suggested to be stoichiometrically linked (Eq. 11; Berner et al., 1970; Heinrich and Reeburgh, 1987), Na-molybdate inhibited sulfate reduction experiments in marine sediments does not show any significant influence on NH_4^+ production, suggesting lack of direct mechanistic link between NH_4^+ production and SO_4^{2-} reduction (Jacobson et al., 1987). This is also obvious from our pore-water data which show steady increase in NH_4^+ concentrations with depth well below the depth of complete sulfate consumption (16 to 19

mbsf). NH_4^+ accumulation with depth also suggests availability of labile organic matter which undergo fermentation to produce CO_2 which fuels methanogenesis explained earlier.

Several processes may lead to ammonium consumption/ adsorption in marine sediments resulting in deviation from a systematic down-depth concentration profile. Lojen et al. (1997) suggested the possibility of assimilation of NH_4^+ by methanogenic archaea. Marked depletion of pore-water NH_4^+ concentrations could also be brought about at the NH_4^+ - SO_4^{2-} transition via lithotrophic and/or organotrophic sulfate reducing-ammonium oxidation pathways (Schrum et al., 2009; Mazumdar et al., 2012). However, we have not observed any marked depletion in NH_4^+ concentrations across the NH_4^+ - SO_4^{2-} transition in Mahanadi basin cores. Pore-water ammonium may also undergo reoxidation (Dalsgaard and Thamdrup, 2002), adsorption-desorption reaction with solid phases like clay, organic particulates and Fe-oxyhydroxides (Boatman and Murray, 1982; Mackin and Aller, 1984).

5.4 Genesis of the sulfate profiles

Pore-water sulfate concentration profiles in marine sediments are strongly coupled to the availability of substrate amenable to sulfate reducers, diffusive/ advective methane flux and depositional conditions (Niewöhner et al., 1998; Zabel and Schulz, 2001; Hensen et al., 2003; Schmidt et al., 2005; Tréude et al., 2005; Kastner et al., 2008; Burdige and Komada, 2011; Malinverno and Pohlmann, 2011; Mazumdar et al., 2012). Relative changes in these factors give rise to sigmoidal, kink, concave-up, concave-down and linear type sulfate concentration trends in marine sediments. Availability of labile organic matter influences the sulfate reduction rates primarily near the sediment water interface, whereas focused sulfate consumption at the SMTZ is primarily controlled by AOM, resulting in two maxima in the sulfate reduction rates as reported by Iversen and Jørgensen (1985) and Tréude et al. (2005). The relative contribution of AOM on the overall sulfate concentration profile as well as the depth integrated sulfate reduction rates depend on the methane flux at the SMTZ. Linear sulfate profiles, high concentration gradient (shallow SMTZ) and high sulfate reduction rates are expected to be coupled with high methane flux (Borowski et al., 1996; Niewöhner et al., 1998; Borowski et al., 1999). The spatial variation in the linearity of sulfate profiles and depths to the SMTZ have been linked to methane hydrate occurrences (Borowski, et al., 1996; Bhatnagar, et al., 2008; Hiruta, et al., 2009). Apparently, the quasi-linear sulfate concentration profiles and high alkalinity at the SMTZ (Fig. 7) recorded from the Mahanadi basin can be linked to high methane flux and AOM. In

addition, enrichment in concentrations of CH₄ and ¹³C of CH₄, coupled with rise in pore water NH₄⁺ concentrations with depth observed at Mahanadi coring sites, suggest accumulation of methane in pore-waters due to progressive degradation of organic matter and subsequent hydrogenotrophy of CO₂ leading to methanogenesis (Eq.6). Methane hydrate crystallized as disseminated layers within the hydrate stability zone when methane concentration exceeded the saturation level at the ambient P-T condition. Low hydrate saturation and presence of only thin disseminated layers suggest absence of upward advective flow of methane from deeper layers into the gas hydrate stability zone (Davie and Buffett, 2001). Markedly close J_{SO4} (10.2-12.8 mmol m²-y⁻¹) recorded in the present study suggest relatively uniform methane flux likely controlled by diffusion dominated flow rather than advection through heterogeneously distributed fault-fracture zones as observed in the Krishna-Godavari basin south of Mahanadi basin (Riedel et al., 2010; Dewangan et al., 2011). The upward diffusion of free gas accumulated at the base of GHSZ is possibly the immediate methane source responsible for the AOM. Factors like enhanced bottom-water temperature, drop in sea level, enhanced sedimentation rate can destabilize the base of GHSZ and subsequent enhancement of diffusive methane flux leading to intensification of AOM. The present bottom water temperature (3.5 to 4.4 °C) and pressure (14.5 to 17 MPa) conditions at the Mahanadi basin sampling sites are well within the range for methane hydrate stability. Due to the stable sea level in the late Holocene (Hashmi et al., 1995), the P-T condition has not shifted noticeably to destabilize the hydrate deposit (Sloan, 1998). However, a sudden increase in sedimentation rate (Fig. 4) in the late Holocene may result in destabilization of the base of hydrate stability zone which can cause recycling of hydrate to methane gas (Hyndman and Davis, 1992; Davie and Buffett, 2001). Modeling studies are required in future for better understanding these factors which control the methane flux variation in Mahanadi basin.

Conclusions

Sediment cores collected from the Mahanadi basin over a water depth of 1429 to 1691 mbsf reveal markedly consistent pore-water sulfate, alkalinity, ammonium and methane concentration profiles. The depth integrated sulfate flux at SMTZ ranges from 10.2 to 12.5 mmol m²-y⁻¹. C₁/(C₂+C₃) hydrocarbon ratios and δ¹³C_{CH4} of headspace gases suggest a microbial origin of methane in the Mahanadi basin. We attribute the complex nature of alkalinity profiles to bicarbonate production via AOM/ organo-clastic degradation and consumption via calcite precipitation. Clustering of data points around the 1:1

line on ($\Delta\text{Ca}+\Delta\text{Alk}$) vs ΔSO_4^{2-} plot suggests a dominant contribution of pore-water bicarbonate via AOM pathway. The quasi-linear sulfate concentration profile and a shallow SMTZ suggest high diffusive methane flux likely originating from the base of gas hydrate stability zone.

Acknowledgment

We thank the directors of CSIR-NIO, NIOT, NCAOR and advisor MOES for supporting this study. Head, oceanography department, and in-charge, on-board operations of IPEV are thanked for providing onboard technical support and facilities. Sincere thanks to students of Goa University, IIT Kharagpur and project scientists of CSIR-NIO, NIOT, PRL and NGRI. Research fellowship from VNJCT to A. Peketi is sincerely acknowledged.

References

- Acharyya, S.K., Basu, P.K., 1993. Toba Ash on the Indian Subcontinent and Its Implications for Correlation of Late Pleistocene Alluvium. *Quaternary Research* 40, 10–19.
- Alperin, M., Reeburgh, W., Whiticar, M., 1988. Carbon and hydrogen isotope fractionation resulting from anaerobic methane oxidation. *Global Biogeochemical Cycles* 2, 279-288.
- Alperin, M.J., Blair N.E., Albert, D.B., Hoehler, T.M., Martens, C.S., 1992. Factors that control the stable carbon isotopic composition of methane produced in anoxic marine sediment. *Global Biogeochemical Cycles* 6, 271-291.
- Berner, R.A., Scott, M.R., Thomlison, C., 1970. Carbonate alkalinity in the pore-waters of the anoxic marine sediments. *Limnology Oceanography* 15, 544-549.
- Berner, R.A., 1978. Sulfate reduction and the rate of deposition of marine sediments. *Earth Planetary Science Letters* 37, 492-498.
- Berner, R.A., 1980. *Early Diagenesis: A Theoretical Approach*. Princeton University Press. Princeton, N.J., 241 pp.
- Bhatnagar, G., Chapman, W.G., Dickens, G.R., Dugan, B., 2008. Sulfate-methane transition as a proxy for average methane hydrate saturation in marine sediments. *Geophysical Research Letters* 35, 1-15.
- Boatman, C.D., Murray, J.W., 1982. Modeling exchangeable NH_4^+ adsorption in marine sediments: process and controls of adsorption. *Limnology Oceanography* 27, 99– 110.

- Boetius, A., Ravenschlag, K., Schubert, C., Rickert, D., Widdel, F., Gieseke, A., Amman, R., Joergensen, B.B., Wittie, U., Pfannkuche, O., 2000. A marine microbial consortium apparently mediating anaerobic oxidation of methane. *Nature* 407, 623–626.
- Borowski, W.S., Paull, C.K., Ussler III, W., 1996. Marine pore-water sulfate profiles indicate in situ methane flux from underlying gas hydrate. *Geology* 24, 655-658.
- Borowski, W.S., Paull, C.K., Ussler III, W., 1999. Global and local variations of interstitial sulfate gradients in deep-water, continental margin sediments: Sensitivity to underlying methane and gas hydrates. *Marine Geology* 159, 131-154.
- Borowski, W.S., Hoehler, T.M., Alperin, M.J., Rodriguez, N.M., Paull, C.P., 2000 Significance of anaerobic methane oxidation in me-rich sediments overlying the blake ridge gas hydrates. In: Paull, C.K., Matsumoto, R., Wallace, P.J., and Dillon, W.P. (Eds.), *Proceedings of the Ocean Drilling Program, Scientific Results* 164, pp.87.
- Brüchert, V., 2004. Physiological and ecological aspects of sulfur isotope fractionation during bacterial sulfate reduction. In: Amend, J.P., Edwards K.J. and Lyons T.W. (Eds.), *Sulfur Biogeochemistry—Past and Present*. GSA Special Paper 379, pp. 1–16.
- Burdige, D., Komada, T., 2011. Anaerobic oxidation of methane and the stoichiometry of remineralization process. *Limnology Oceanography* 56, 1781-1796.
- Burke, K., Dewey, F.J., 1973. Plume generated triple junctions: key indicator in applying plate tectonic to old rocks. *Journal of Geology* 8, 406–439.
- Canfield, D.E., 1989. Sulfate reduction and oxic respiration in marine sediments: implications from organic carbon preservation in euxinic environments. *Deep Sea Research* 36, 121-138.
- Canfield, D., 1991. Sulfate reduction in deep sea sediments. *American Journal Science* 291, 177-188.
- Canfield, D.E., 2001. Biogeochemistry of sulfur isotopes. *Reviews in Mineralogy and Geochemistry* 43, 607-636.
- Canfield, D.E., Kristensen, E., Thamdrup, B., 2005a. The methane cycle. In: Canfield, D.E., Kristensen, E. and Thamdrup, B. (Eds.), *Advances in Marine Biology. Aquatic Geomicrobiology* 48, pp. 383-418.
- Canfield, D.E., Kristensen, E., Thamdrup, B., 2005b. The sulfur cycle. In: Canfield, D.E., Kristensen, E. and Thamdrup, B. (Eds.), *Advances in Marine Biology. Aquatic Geomicrobiology* 48, pp. 313-381.
- Canfield, D.E., Olesen, C.A., Cox, R.P., 2006. Temperature and its control of isotope fractionation by a sulfate-reducing bacterium. *Geochimica et Cosmochimica Acta* 70, 548-561.

- Chen, Y., Ussler III, W., Haflidason, H., Lepland, A., Rise, L., Hovland, M., Hjelstuen, B.O., 2010. Sources of methane inferred from pore-water $\delta^{13}\text{C}$ of dissolved inorganic carbon in Pockmark G11, offshore Mid-Norway. *Chemical Geology* 275, 127-138.
- Claypool, G., 2004. Ventilation of marine sediments indicated by depth profiles of pore water sulfate and $\delta^{34}\text{S}$. *The Geochemical Society Special Publication* 9, 59-65.
- Cline, J.D., 1969. Spectrophotometric determination of hydrogen sulfide in natural waters. *Limnology Oceanography* 14, 454-458.
- Coffin, R., Pohlman, J., Gardner, J., Downer, R., Wood, W., Hamdan, L., Walker, S., Plummer, R., Gettrust, J., Diaz, J., 2007. Methane hydrate exploration on the mid Chilean coast: A geochemical and geophysical survey. *Journal of Petroleum Science and Engineering* 56, 32-41.
- Collett, T., Riedel, M., Cochran, J., Boswell, R., Presley, J., Kumar, P., Sathe, A., Sethi, A., Lall, M., Sibal, V., 2008. The NGHP Expedition 01 Scientists. Indian National Gas Hydrate Program Expedition 01 Initial Reports.
- Conrad, R., 2005. Quantification of methanogenesis pathways using stable carbon isotope signatures: a review and a proposal. *Organic Geochemistry* 36, 739-752.
- Dalsgaard, T., Thamdrup, B., 2002. Factors controlling anaerobic ammonium oxidation with nitrite in marine sediments. *Applied Environmental Microbiology* 68, 3802-3808.
- Davie, M.K., Buffett, B.A., 2001. A numerical model for the formation of gas hydrate below the seafloor. *Journal of Geophysical Research: Solid Earth* 106, 497-514.
- Detmers, J., Bruchert, V., Habicht, K., Kuever, J., 2001. Diversity of sulfur isotope fractionations by sulfate-reducing prokaryotes. *Applied Environmental Microbiology* 67, 888-894.
- Dewangan, P., Sriram, G., Ramprasad, T., Ramana, M., Jaiswal, P., 2011. Fault system and thermal regime in the vicinity of site NGHP-01-10, Krishna-Godavari basin, Bay of Bengal. *Marine and Petroleum Geology* 28, 1899-1914.
- Dickens, G.R., Paull, C.K., Wallace, P., ODP Leg 164 Scientific Party 1997. Direct measurement of in situ methane quantities in a large gas-hydrate reservoir. *Nature* 385, 426-428.
- Fairbanks, R.G., Mortlock, R.A., Chiu, T.C., Cao, L., Kaplan, A., Guilderson, T.P., Fairbanks, T.W., Bloom, A.L., Grootes, P.M., Nadeau, M.J., 2005. Radiocarbon calibration curve spanning 0 to 50,000 years BP based on paired $^{230}\text{Th}/^{234}\text{U}/^{238}\text{U}$ and ^{14}C dates on pristine corals. *Quaternary Science Reviews* 24, 1781-1796.
- Galimov, E.M., 2006. Isotope organic geochemistry. *Organic Geochemistry* 37, 1200-1262.

- Garcia, J.L., Patel, B.K.C., Ollivier, B., 2000. Taxonomic, phylogenetic, and ecological diversity of methanogenic Archaea. *Anaerobe* 6, 205-226.
- Gélinas, Y., Baldock, J.A., Hedges, J.I., 2001. Organic carbon composition of marine sediments: effects of oxygen exposure on oil generation potential. *Nature* 294, 145-148.
- Gieskes, J.M., 1974. Interstitial water studies, Leg 25. In Simpson, E.S.W., Schlich, R., et al., *Init. Repts. DSDP, 25*: Washington, DC (U.S. Govt. Printing Office), 361–394.
- Gieskes, J. M., Peretsman, G., 1986. Water chemistry procedures aboard *JOIDES Resolution*—some comments. *ODP Tech. Note*, 5.
- Gieskes, J.M., Gamo, T., Brumsack, H., 1991. Chemical methods for interstitial water analysis aboard JOIDES Resolution: College Station, Texas, Ocean Drilling Program Technical Note no. 15, pp. 60.
- Goldhaber, M., Kaplan, I., 1975. Controls and consequences of sulfate reduction rates in recent marine sediments. *Soil Science* 119, 42-55.
- Hallam, S.J., Putnam, N., Preston, C.M., Detter, J.C., Rokhsar, D., Richardson, P.M., DeLong, E.F., 2004. Reverse methanogenesis: testing the hypothesis with environmental genomics. *Science* 305, 1457–1462.
- Harrison, A.G., Thode, H.G., 1958. Mechanism of the bacterial reduction of sulphate from isotopic fractionation studies. *Transactions Faraday Society* 54, 84-92.
- Hartnett, H.E., Keil, R.G., Hedges, J.L., Devol, A.H., 1998. Influence of oxygen exposure time on organic carbon preservation in continental margin sediments. *Nature* 391, 572-574.
- Hashimi, N.H., Nigam, R.; Nair, R.R.; Rajagopalan, G, 1995. Holocene sea level fluctuations on western Indian continental margin: An update. *Journal of the Geological Society of India* 46, 157-162.
- Hedges, J.I., Keil, R.G., 1995. Sedimentary organic matter preservation: an assessment and speculative synthesis. *Marine Chemistry* 49, 81-115.
- Heinrich, S.M., Reeburgh, W.S., 1987. Anaerobic mineralization of marine sediment organic matter: rates and the role of anaerobic processes in the oceanic carbon economy. *Geomicrobiology Journal* 5, 191-237.
- Hensen, C., Zabel, M., Pfeifer, K., Schwenk, T., Kasten, S., Riedinger, N., Schulz, H.D., Boetius, A., 2003. Control of sulfate pore-water profiles by sedimentary events and the significance of anaerobic oxidation of methane for burial of sulfur in marine sediments. *Geochimica Cosmochimica Acta* 67, 2631–2647.

- Hinrichs, K.U., Boetius, A.B., 2002. The anaerobic oxidation of methane: new insights in microbial ecology and biogeochemistry. In: Wefer, G., Billet, D., Hebbeln, D., Jørgensen, B.B., Schlüter, M. and van Weering, T. (Eds.), *Ocean Margin Systems* Springer-Verlag, pp. 457–477.
- Hiruta, A., Snyder, G. T., Tomaru, H., Matsumoto, R., 2009. Geochemical constraints for the formation and dissociation of gas hydrate in an area of high methane flux, eastern margin of the Japan Sea. *Earth and Planetary Science Letters* 279, 326-339.
- Hofstetter, T., Schwarzenbach, R and Bernasconi, S., 2008. Assessing Transformation Processes of Organic Compounds Using Stable Isotope Fractionation. *Environ. Sci. Technol.* 42, 7737–7743.
- Hyndman, R. D., Davis, E.E., 1992, A mechanism for the formation of methane hydrate and seafloor bottom-simulating reflection by vertical fluid expulsion. *Journal of Geophysical Research* 97, 7025-7041.
- Hyndman, R.D., Spence, G.D., 1992. A Seismic Study of Methane Hydrate Marine Bottom Simulating Reflectors. *Journal of Geophysical Research* 97, 6683-6698.
- Iversen, N., Jørgensen, B.B., 1985. Anaerobic methane oxidation rates at the sulfate-methane transition in marine sediment from Kattegat and Skagerrak (Denmark). *Limnology and Oceanography* 30, 944-955.
- Iversen, N., Jørgensen, B.B., 1993. Diffusion coefficients of sulfate and methane in marine sediments: Influence of porosity. *Geochimica et Cosmochimica Acta* 57, 571–578.
- Jacobson, M.E., Mackin, J.E. Capone, D.G., 1987. Ammonium Production in Sediments Inhibited with Molybdate: Implications for the Sources of Ammonium in Anoxic Marine Sediments. *Applied and Environmental Microbiology* 53, 2435-2439.
- Jagannathan, C.R., Ratnam, C., Baishya, N.C., Das Gupta, U., 1983. Geology of the Offshore Mahanadi Basin. *Petroleum Asia Journal* 6, 101-104.
- Jarrell, K.F., 1985. Extreme oxygen sensitivity in methanogenic archaeobacteria. *Bioscience* 35, 298-302.
- Jin, Q., Bethke, C.M., 2009. Cellular energy conservation and the rate of microbial sulfate reduction, *Geology*, 37, 1027–1030.
- Jørgensen, B., 1977. The sulfur cycle of a coastal marine sediment (Limfjorden, Denmark). *Limnology and Oceanography* 22, 814-832.
- Jørgensen, B., 1982. Mineralization of organic matter in the sea bed—the role of sulphate reduction. *Nature* 296, 643-645.
- Kasten, S., Jørgensen, B.B., 2000. Sulfate Reduction in Marine Sediments. In: Schulz, H.D. and Zabel, M.(Eds.), *Marine Geochemistry*. Springer, p.455.

- Kastner, M., Claypool, G., Robertson, G., 2008. Geochemical constraints on the origin of the pore fluids and gas hydrate distribution at Atwater Valley and Keathly Canyon, northern Gulf of Mexico. *Marine and Petroleum Geology* 25, 86-872.
- Knittel, K., Boetius, A., 2009. Anaerobic oxidation of methane: progress with as unknown process. *Annual Review of Microbiology* 63, 311-334.
- Koho, K.A., Nierop, K.G.J., Moodley, L., Middelburg, J.J., Pozzato, L., Soetaert, K., Van der Plicht, J. Reichart, G.J., 2013. Microbial bioavailability regulates organic matter preservation in marine sediments *Biogeosciences* 10, 1131–1141.
- Koroleff, F., 1976. Determination of $\text{NH}_4^+\text{-N}$. In: *Method of seawater analysis*. Grasshoff, K.(Eds.), Verlag Chemie, Weinheim, pp 126-133.
- Kristensen, E., 2000. Organic matter diagenesis at the oxic/anoxic interface in coastal marine sediments, with emphasis on the role of burrowing animals. *Hydrobiologia* 426, 1-24.
- Krüger, M., Meyerdierks, A., Glöckner, F.O., Amann, R., Widdel, F., Kube, M., Reinhardt, R., Kahnt, J., Böcher, R., Thauer, R.K., 2003. A conspicuous nickel protein in microbial mats that oxidise methane anaerobically. *Nature* 426, 878–881.
- Kuznetsov, S.I., 1975. *The Microflora of Lakes and its Geochemical Activity*. University of Texas Press, Austin, p.503
- Kvenvolden, K., 1993. Gas hydrates-Geological perspective and global change. *Reviews of Geophysics* 31, 173–187.
- Kvenvolden, K.A., Lorenson, T.D., 2001. The global occurrence of natural gas hydrates. In: Paull, C.K., and Dillon, W.P. (Eds.), *Natural Gas Hydrates: Occurrence, Distribution, and Detection*, AGU, Washing, D. C., 3-18.
- Lashof, D.A., Ahuja, D.R., 1990. Relative contributions of greenhouse gas emissions to global warming. *Nature* 344, 529-531.
- Lojen, S., Ogrinc, N. Dolenc, T., 1997. Carbon and Nitrogen stable isotope fractionation in the sediment of lake bleed (Slovenia). *Water, air and soil pollution* 99, 315-323.
- Li, Y.H., Gregory, S., 1974. Diffusion of ions in sea water and in deep sea sediments. *Geochimica et Cosmochimica Acta* 38, 703-714.
- Mackin, J.E., Aller, R.C., 1984. Ammonium adsorption in marine sediments. *Limnology and Oceanography* 29, 250-257.
- Madigan, M., Martinko, J., Parker, J., 2000. *Brock Biology of Microorganisms*, Prentice-Hall, New Jersey, 991p.

- Malinverno, A., Pohlman, J.W., 2011. Modeling sulfate reduction in methane hydrate-bearing continental margin sediments: Does a sulfate-methane transition require anaerobic oxidation. *Geochemistry, Geophysics, Geosystems* 12, 1-18.
- Martens, C.S., Berner, R., 1974. Methane production in the interstitial waters of sulfate-depleted marine sediments. *Science* 185, 1167-1169.
- Mazumdar, A., Joao, H.M., Peketi, A. Dewangan, P., Kocherla, M., Joshi, R.K., Rarnprasad, T., 2012. Geochemical and geological constraints on the composition of marine sediment pore fluid: Possible link to gas hydrate deposits. *Marine and Petroleum Geology* 38, 35-52.
- Megonigal, J.P., Hines, M.E., Visscher, P.T., 2003. Anaerobic Metabolism: Linkages to Trace Gases and Aerobic Processes. In *Treatise on Geochemistry*. Holland, H.D. and Turekian K.K.(Eds.) Biogeochemistry 8, pp. 317-424.
- Milkov A.V., Claypool G.E, Lee, Y., Sassen, R., 2005. Gas hydrate systems at Hydrate Ridge offshore Oregon inferred from molecular and isotopic properties of hydrate-bound and void gases. *Geochimica et Cosmochimica Acta* 69, 1007-1026.
- Milucka, J., Ferdelman, T.G., Polerecky, L., Franzke1, D., Wegener, G., Schmid, M., Lieberwirth, I., Wagner, M., Widdel, F., Kuypers., M.M.M., 2012. Zero-valent sulphur is a key intermediate in marine methane oxidation. *Nature* 491, 541-546
- Mohapatra, P., 2006. Sequence stratigraphic approach for Identification of hydrocarbon plays in Mahanadi offshore basin, 6th International Conference & Exposition on Petroleum Geophysics, pp.672-677.
- Niewohner, C., Hensen, C., Kasten, S., Zabel., M., Schulz. H.D., 1998. Deep sulfate reduction completely mediated by anaerobic methane oxidation in sediments of the upwelling area off Namibia. *Geochimica et Cosmochimica Acta* 62, 455-464.
- Ninkovitch, D., 1979. Distribution, age and chemical composition of tephra layers in the deep-sea sediments off western Indonesia. *Journal of Volcanology and Geothermal Research* 5, 67-86.
- Orphan, V.J., House, C.H., Hinrichs, K.-U., McKeegan, K.D., DeLong, E.F., 2001. Methane consuming Archaea revealed by directly coupled isotopic and phylogenetic analysis. *Science* 293, 484-487.
- Paull, C.K., Ussler III, W., 2001. History and significance of gas sampling during DSDP and ODP drilling associated with gas hydrates. In: Paull, C.K. and Dillon, W. P.(Eds.). *Natural Gas Hydrates: Occurrence, Distribution and Detection*. AGU, Washington, DC, pp. 3-65.
- Pereira, I.A.C., Ramos, A.R., Grein, F., Coimbra, M., Marues, M. C., da Silva, S. M., Veneslau, S. S., 2011, A comparative genomic analyses of enrgy metabolism in sulfafte reducing bacteria and archaea. *Frontiers in microbiology*, 2, 1-22.

- Rabus, R., Hansen, T., Widdel, F., 2007. "Dissimilatory sulfate and sulfur reducing prokaryotes, in The Prokaryotes, ed. M. Dworkin (New York: Springer -Verlag), 659-768.
- Reeburgh, W.S., 2007. Ocean methane biogeochemistry. *Chemical Reviews* 107, 486-513.
- Riedel, M., Collett, T.S., Kumar, P., Sathe, A.V., Cook, A., 2010. Seismic imaging of a fractured gas hydrate system in the Krishna-Godavari Basin offshore India. *Marine and Petroleum Geology* 27, 1476-1493.
- Rontani, J.F., Charriere, B., Petit, M., Vaultier, F., Heipieper, H.J., Link, H., Chaillou, G., Sempér'e, R., 2012. Degradation state of organic matter in surface sediments from the Southern Beaufort Sea: a lipid approach. *Biogeosciences* 9, 3513–3530.
- Sayles, FL., Manheim, ET., Waterman, L.S., 1973. Interstitial water studies on small core samples, Leg 15. In Heezen, B.C., MacGregor, I.D., et al., *Init. Repts. DSDP*, 20: Washington (U.S. Govt. Printing Office), 783-804.
- Scheller, S., Goenrich, M., Boecher, R., Thauer, R.K., Jaun, B., 2010. The key nickel enzyme of methanogenesis catalyses the anaerobic oxidation of methane. *Nature* 465, 606-608.
- Schönheit, P., Keweloh, H., Thauer, R.K., 1981. Factor F₄₂₀ degradation in *Methanobacterium thermoautotrophicum* during exposure to oxygen. *FEMS Microbiology Letter* 12, 347–349.
- Schmidt, M., Hensen, C., Mörz, T., Müller, C., Grevemeyer, I., Wallmann, K., Mau, S., Kaul, N., 2005. Methane hydrate accumulation in "Mound 11" mud volcano, Costa Rica forearc. *Marine Geology* 216, 83-100.
- Schrum, H.N., Spivack, A.J., Kastner, M., D'Hondt, S., 2009. Sulfate-reducing ammonium oxidation: A thermodynamically feasible metabolic pathway in subseafloor sediment. *Geology* 37, 939-942.
- Schulz, H.D., Zabel, M., 2000. *Marine Geochemistry*. Springer, Berlin, Heidelberg, New York, p 455.
- Singh, L., 2008. Mahanadi Basin (Mahanadi -NEC basin) Oil and gas fields of India, Indian Petroleum publishers, Dehradun, India. 325-346.
- Sloan, E.D. Jr., 1998, *Clathrate hydrates of natural gases* (2nd edition), 730 pp., New York, Marcel Dekker Inc.
- Solomon, E.A., Spivack, A., Kastner, M., Torres, M., Borole, D.V., Robertson, G., Das, H.C., 2008. Hydrogeochemical and structural controls on heterogeneous gas hydrate distribution in the K-G basin offshore, India. In *Proceedings of the 6th International Conference on Gas Hydrates (ICGH 2008)*, Vancouver, British Columbia, Canada.
- Sørensen, J., Christensen, D., Jørgensen, B.B., 1981. Volatile Fatty Acids and Hydrogen as Substrates for Sulfate-Reducing Bacteria in Anaerobic Marine Sediment. *Applied Environmental Microbiology* 42, 5–11.

- Subrahmanyam, V., Subrahmanyam, A.S., Murty, G.P.S., Murthy, K.S.R. 2008. Morphology and tectonics of Mahanadi Basin, northeastern continental margin of India from geophysical studies. *Marine Geology* 253, 63–72.
- Tréude, T., Niggemann, J., Kallmeyer, J., Wintersteller, P., Schubert, C.J., Boetius, A., Jørgensen, B.B., 2005. Anaerobic oxidation of methane in the sulfate–methane transition along the Chilean continental margin. *Geochimica et Cosmochimica Acta* 69, 2767–2779.
- Ussler III, W., Paull, C.K., 2008. Rates of anaerobic oxidation of methane and authigenic carbonate mineralization in methane-rich deep-sea sediments inferred from models and geochemical profiles. *Earth and Planetary Science Letters* 266, 271–287.
- Valentine, D.L., Reeburgh, W.S., 2000. New perspectives on anaerobic methane oxidation. *Environmental Microbiology* 2, 477–484.
- Wall, J.D., Arkin, A.P., Balci, N.C., Rapp-Giles, B., 2008. Genetics and Genomics of sulfate respiration. In: *Desulfovibrio*, in Dahl, C. and Friedrich, C.G. (Eds), *Microbial sulfate metabolism*, 1–12., Springer-Verlag.
- Wallmann, K., Aloisi, G., Haeckel, M., Tishchenko, P., Pavlova, G., Greinert, J., Kutterolf, S., Eisenhauer, A., 2008. Silicate weathering in anoxic marine sediments. *Geochimica et Cosmochimica Acta* 72, 3067–3090.
- Walker C.B., Redding-Johanson A.M., Baidoo E.E., Rajeev L., He, Z., Hendrickson, E.L., Joachimiak, M, P, Stolyar, S., Leigh, J.A., Zhou J, Keasling J.D., Mukhopadhyay A., Stahl D.A., 2012. Functional responses of Methanogenic archaea to syntrophic growth, *The ISME Journal* 6, 2045–2055.
- Westrich, J.T., Berner, R.A., 1984. The role of sedimentary organic matter in bacterial sulfate reduction: The G model tested. *Limnology and oceanography* 29, 236–249.
- Westrich, J.T., Berner, R.A., 1988. The effect of temperature on rates of sulfate reduction in marine sediments. *Geomicrobiology Journal* 6, 99–117.
- Whiticar, M.J. Faber, E., 1986. Methane oxidation in sediment and water column environments - Isotope evidence. *Organic Geochemistry* 10, 759–768.
- Whiticar, M.J., 1999. Carbon hydrogen isotope systematics of bacterial formation and oxidation of methane. *Chemical Geology* 161, 291–314.
- Whiticar, M.J., 2002. Diagenetic relationships of methanogenesis, nutrients, acoustic turbidity, pockmarks and freshwater seepages in Eckernförde Bay, *Marine Geology* 182, 29–53.
- Zabel, M., Schulz, H.D., 2001. Importance of submarine landslides for non-steady state conditions in pore water system-lower Zaire (Congo) deep-sea fan. *Marine Geology* 176, 87–99.

Figures and Tables captions

Figure 1. Bathymetry map of the study area. The core locations of JOIDES and Marion Dufresne are represented by 'J' and 'M', respectively. The regional sub-bottom profiles crossing the cores MD161-19 and MD161-27 are shown on the bathymetry map. The inset shows the zoom-out of the study area.

Figure 2. Regional SBP data across the cores MD161-27 and MD161-19 are shown in Fig. 2a and Fig. 2b, respectively. The nearest projection of MD161-25 on the SBP data will be close to the location of MD161-19. The approximate depth (msl) is estimated assuming a constant velocity of 1500 m/s for the water column.

Figure 3. Multi-channel seismic (MCS) data across the Site NGHP-01-19 (modified after Collett et al., 2008) highlighting the presence of BSR and free gas below the BSR in the study area.

Figure 4. Age-depth model for MD161-19.

Figure 5. TOC concentration variation with depth below seafloor.

Figure 6. Ammonium concentration variation with depth below seafloor.

Figure 7. Sulfate, alkalinity and methane concentration profiles. The second bracket indicates the approximate location and thickness of the SMTZ.

Figure 8. Pore-water calcium concentrations and total alkalinity (TA) profiles.

Figure 9. Cross plot of $(\Delta\text{Ca}+\Delta\text{Alk})$ vs. ΔSO_4^{2-} .

Figure 10. Carbon isotope ratios of headspace CO_2 and CH_4 gases.

Figure 11. Cross plot of $\text{C1}/(\text{C2}+\text{C3})$ and carbon isotope ratios of headspace CH_4 .

Table-1. Concentrations and isotope ratios of various dissolved components in the pore-waters and head space gases. nd= not detectable.

Table-2. Total organic carbon concentration.

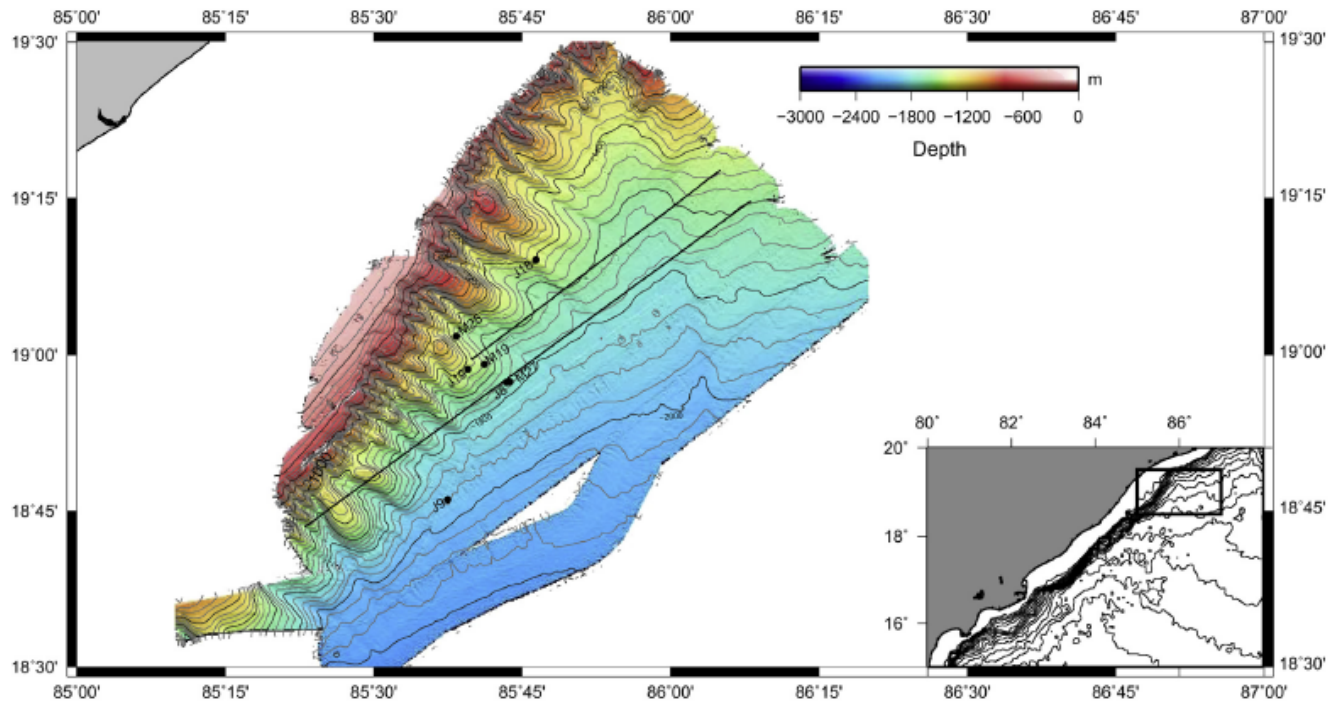


Figure 1. Bathymetry map of the study area. The core locations of JOIDES and Marion Dufresne are represented by 'J' and 'M', respectively. The regional sub-bottom profiles crossing the cores MD161-19 and MD161-27 are shown on the bathymetry map. The inset shows the zoom-out of the study area.

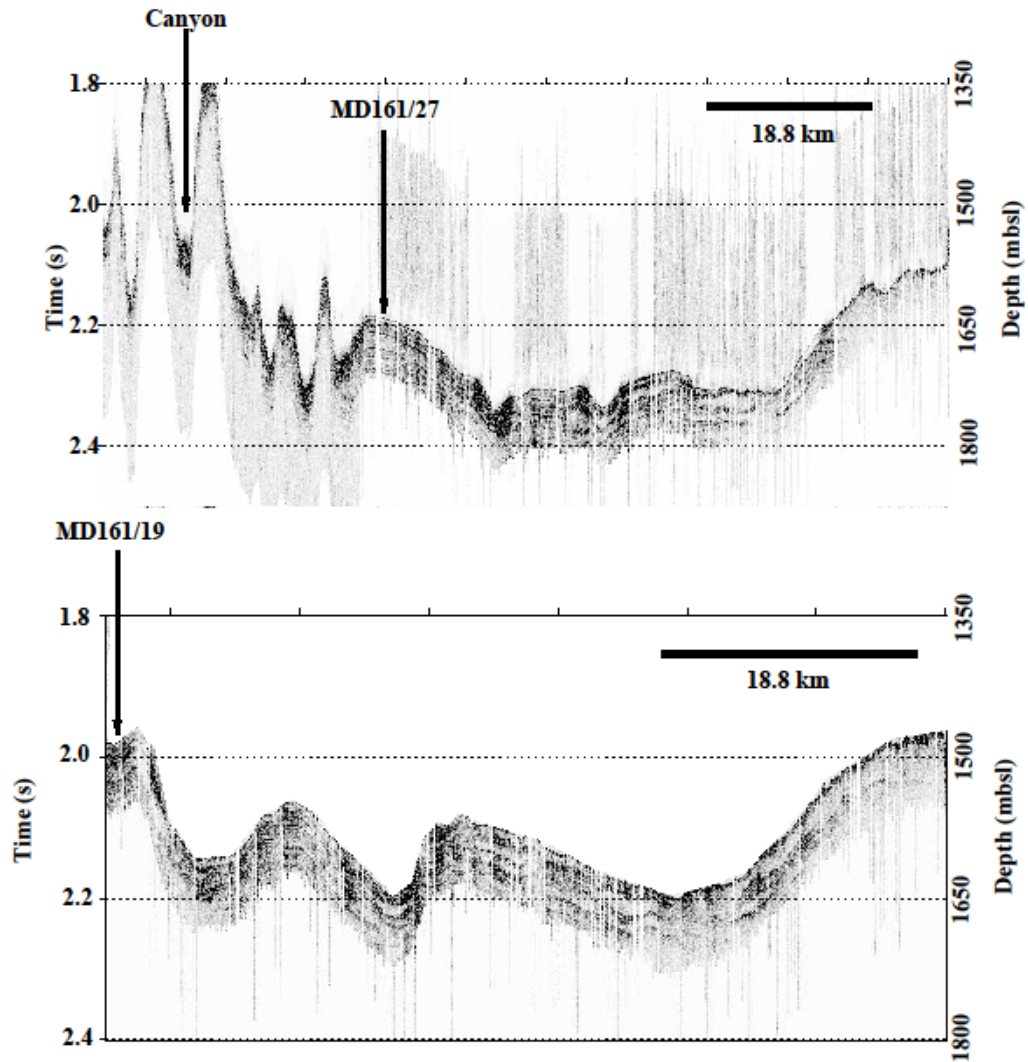


Figure 2. Regional SBP data across the cores MD161-27 and MD161-19 are shown in Fig. 2a and Fig. 2b, respectively. The nearest projection of MD161-25 on the SBP data will be close to the location of MD161-19. The approximate depth (msl) is estimated assuming a constant velocity of 1500 m/s for the water column.

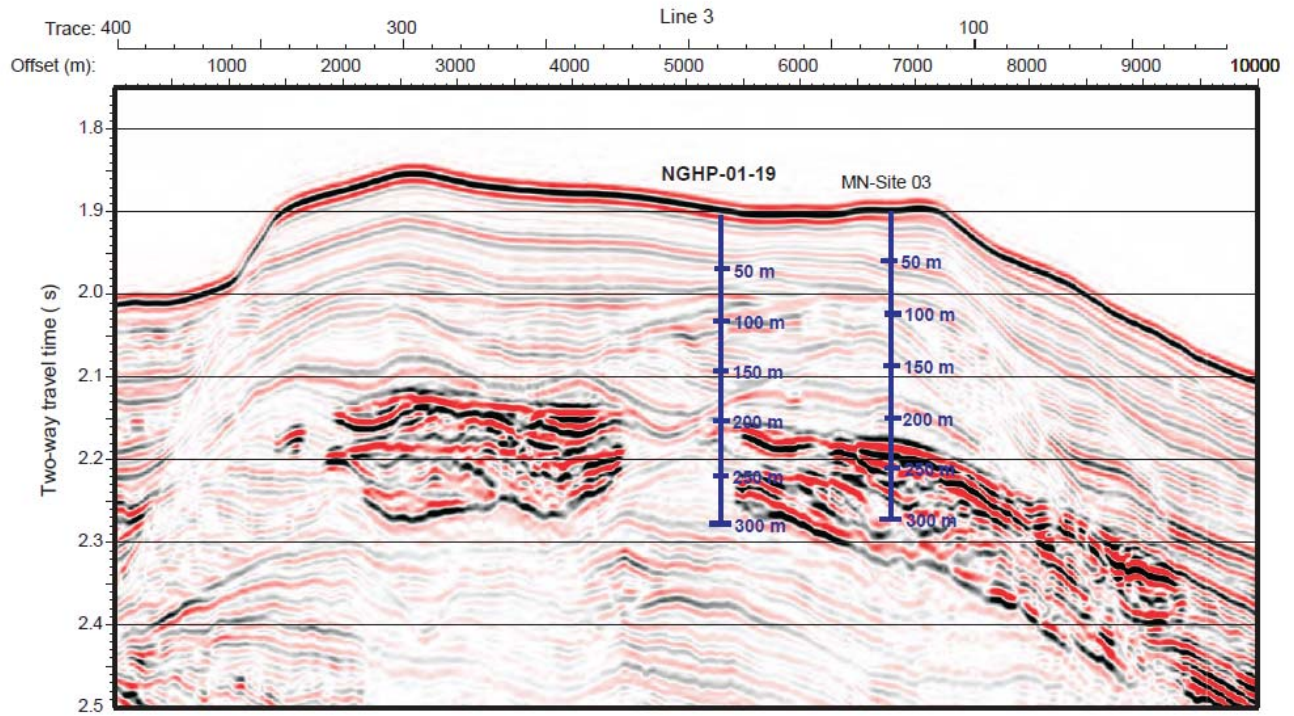


Figure 3. Multi-channel seismic (MCS) data across the Site NGHP-01-19 (modified after Collett et al., 2008) highlighting the presence of BSR and free gas below the BSR in the study area.

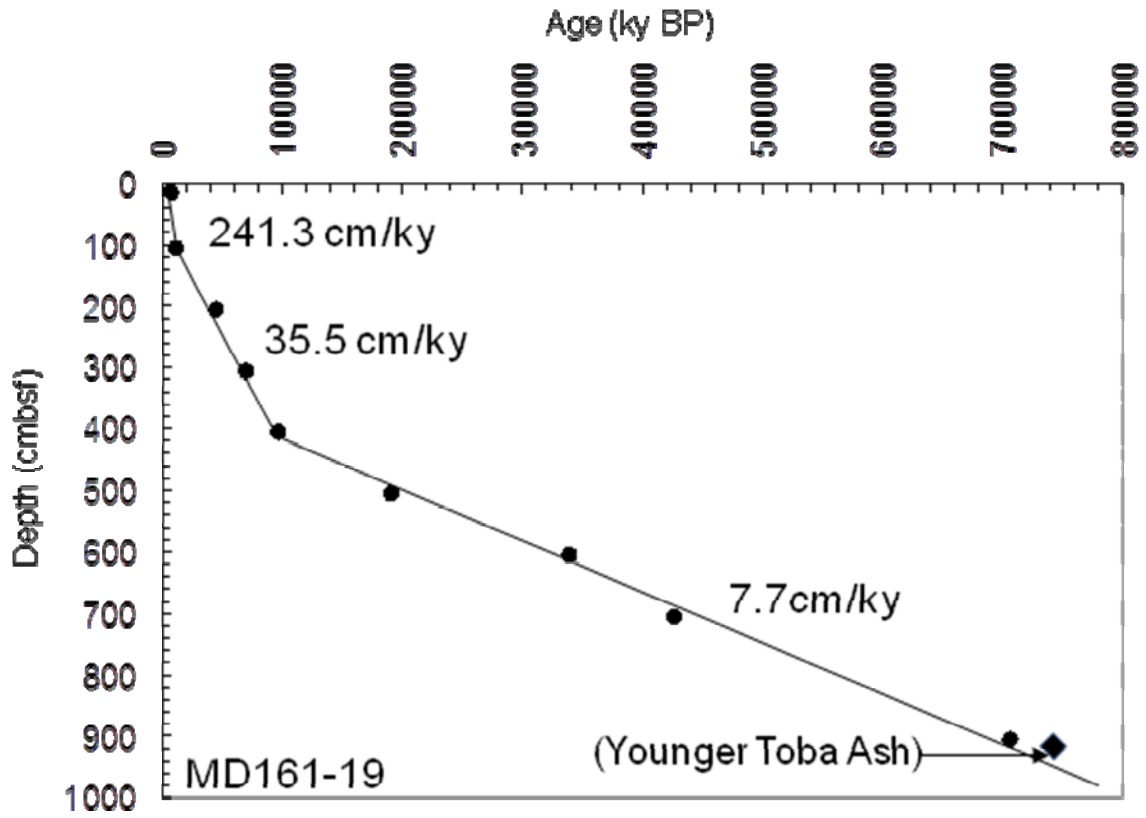


Figure 4. Age-depth model for MD161-19

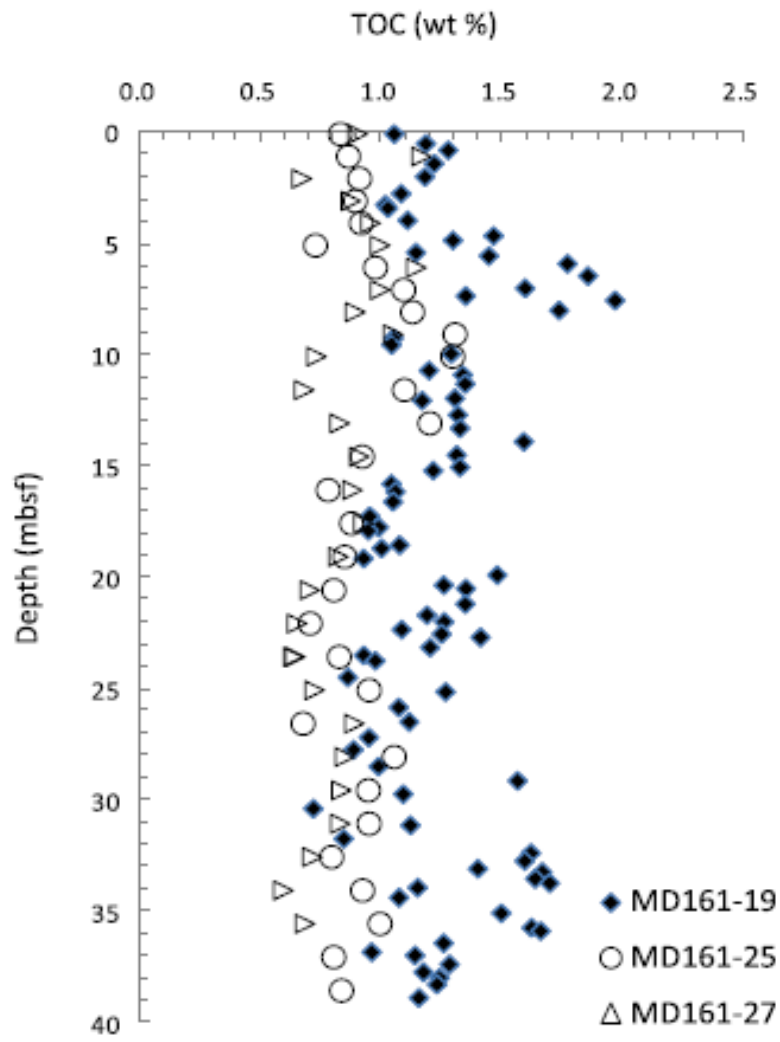


Figure 5. TOC concentration variation with depth below seafloor

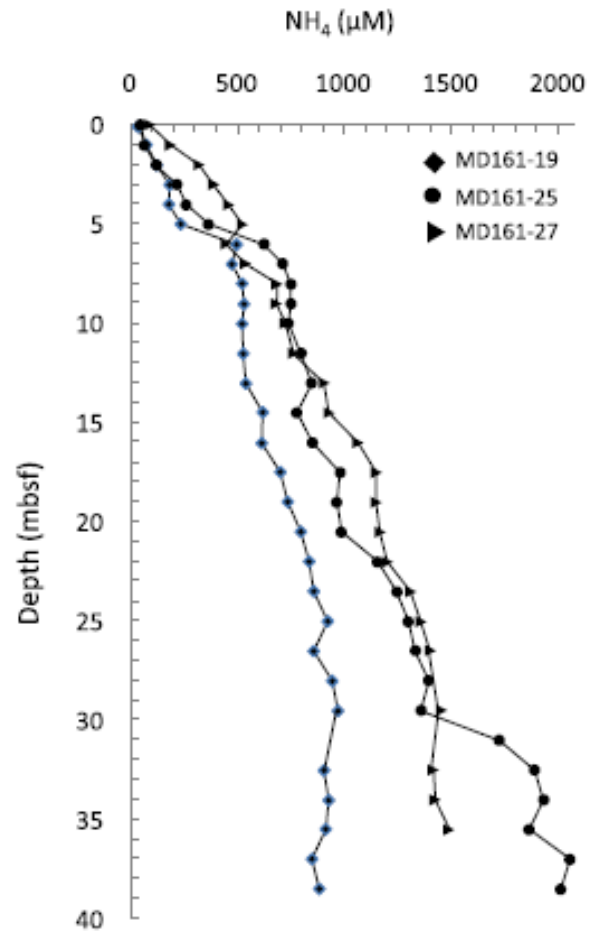


Figure 6. Ammonium concentration variation with depth below seafloor.

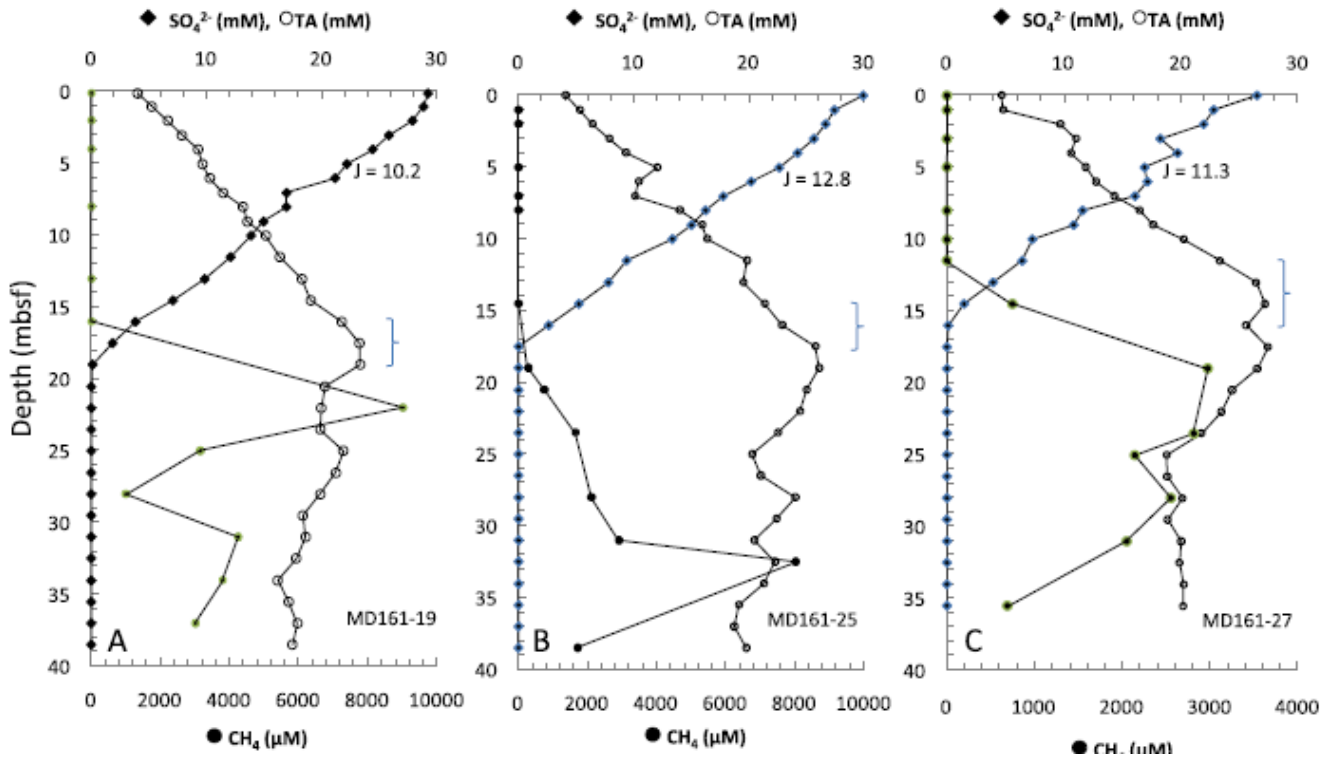


Figure 7. Sulfate, alkalinity and methane concentration profiles. The second bracket indicates the approximate location and thickness of the SMTZ.

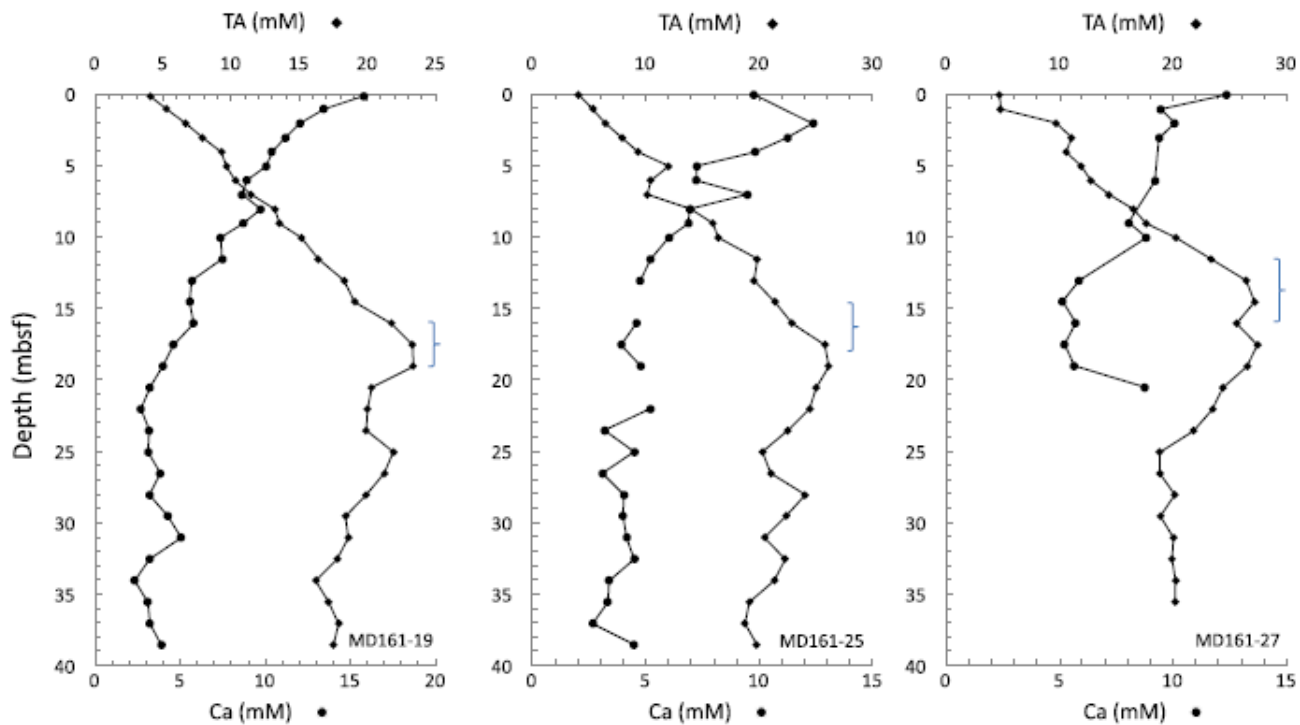


Figure 8. Pore-water calcium concentrations and total alkalinity (TA) profiles.

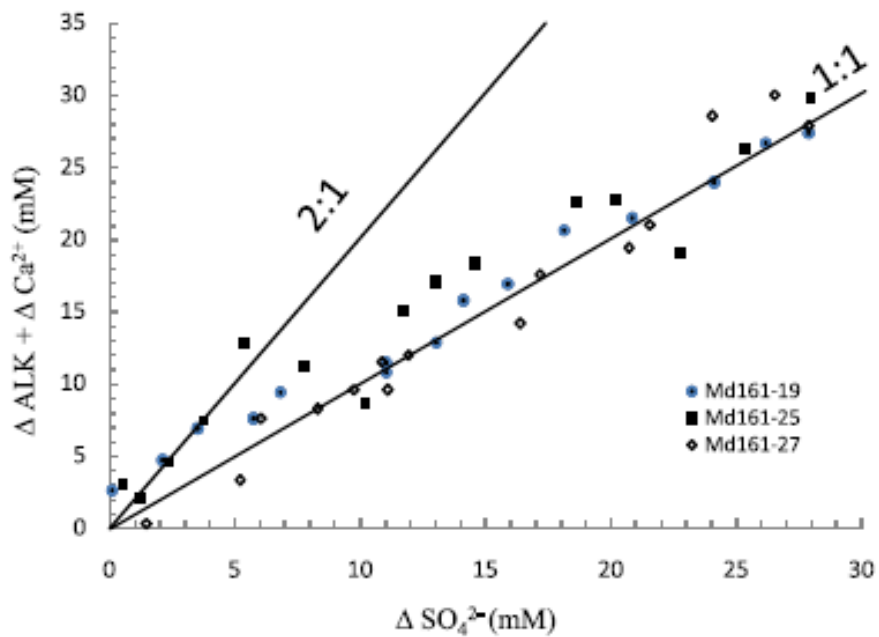


Figure 9. Cross plot of $(\Delta \text{Ca} + \Delta \text{Alk})$ vs. ΔSO_4^{2-} .

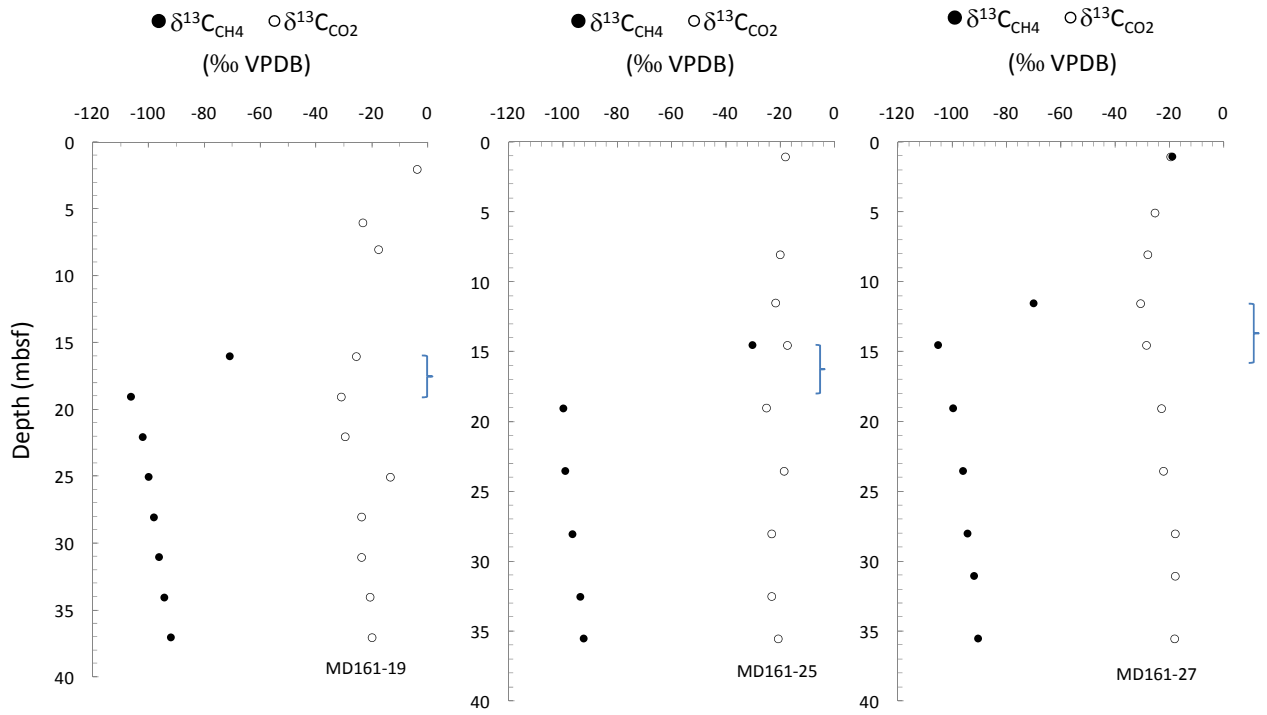


Figure 10. Carbon isotope ratios of headspace CO₂ and CH₄ gases

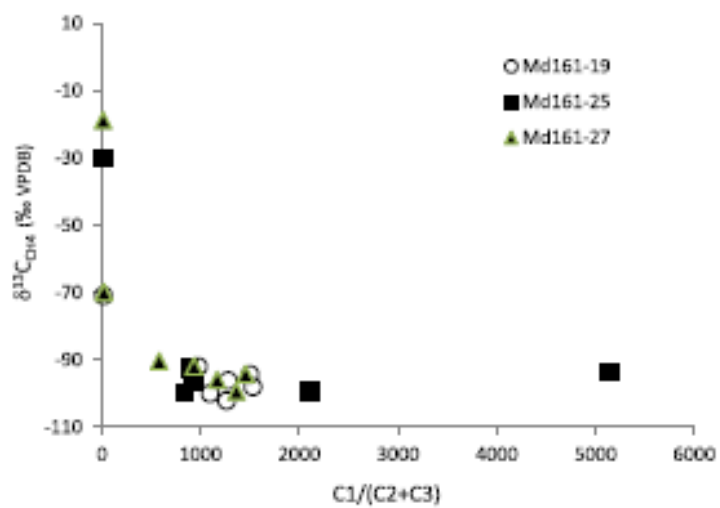


Figure 11. Cross plot of C₁/(C₂+C₃) and carbon isotope ratios of headspace CH₄.

Table-1. Concentrations and isotope ratios of various dissolved components in the pore-waters and head space gases. nd= not detectable.

MD -161-19	Depth (mbsf)	SO4 (mM)	Alk (mM)	NH4 (μ M)	CH4 (μ M)	C1/C2+C3	$\delta^{13}\text{C}_{\text{CH}_4}$	$\delta^{13}\text{C}_{\text{CO}_2}$	Porosity (%)	Ca (mM)	Mg (mM)
							‰ (VPDB)	‰ (VPDB)			
water depth = 1480 m	0.15	29.3	4.05	35.5	3.8	2.7			72.8	15.8	60.0
Long: 18 59.1020N	1.055	28.9	5.25	77.1					77.2	13.4	62.0
Lat: 85 41.1669E	2.055	27.9	6.65	122.4	2.9	5.2		-3.9	76.4	12.0	65.1
Sea bottom T= 4.4 °C	3.055	25.9	7.9	183.6					71.9	11.2	64.0
	4.055	24.5	9.3	181.2	3.8	2.7			71.1	10.4	59.6
	5.055	22.2	9.65	237.5					75.1	10.1	63.4
	6.055	21.2	10.3	495.7		9.6		-23.1		8.9	59.6
	7.055	16.9	11.45	477.4					70.2	8.6	58.2
	8.055	16.9	13.2	521.4	0.8	13.0		-17.6	71.7	9.7	70.7
	9.055	14.9	13.55	531.2					65.5	8.7	68.2
	10.055	13.9	15.15	521.4		8.3				7.4	55.5
	11.55	12.1	16.4	526.3						7.5	56.3
	13.055	9.9	18.3	539.8	3.4	6.7			70.1	5.7	64.7
	14.55	7.1	19.05	616.9					77.9	5.6	56.6
	16.055	3.9	21.75	613.2	3.5	15.1	-70.9	-25.6	55.5	5.8	61.1
	17.55	1.8	23.3	701.3					65.5	4.6	53.8
	19.055	0.1	23.35	734.4			-106.4	-30.8		4.0	52.7
	20.55	nd	20.3	796.8					57.8	3.2	66.1
	22.055	nd	20	837.2	9017.6	1261.9	-102.1	-29.5	66.1	2.7	50.6
	23.55	nd	19.9	855.6					57.8	3.2	51.8
	25.055	nd	21.9	921.7	3148.5	1095.4	-100.0	-13.3	68.4	3.1	49.2
	26.55	nd	21.25	855.6					65.9	3.8	52.7
	28.055	nd	19.9	943.7	993.8	1527.9	-98.0	-23.6	64.2	3.2	47.3

29.55	nd	18.4	969.4						64.0	4.3	49.3
31.055	nd	18.6		4255.2	1278.1	-96.1	-23.6		68.0	5.1	73.6
32.55	nd	17.8	907.0						64.8	3.2	54.5
34.055	nd	16.2	925.3	3797.9	1500.4	-94.3	-20.7		63.7	2.3	45.8
35.55	nd	17.15	914.3						65.9	3.1	47.0
37.055	nd	17.9	848.2	3008.0	976.1	-92.0	-19.8		63.0	3.2	44.4
38.55	nd	17.5	884.9						64.1	3.9	45.3

MD161-25	Depth (mbsf)	SO4 (mM)	Alk (mM)	NH4 (μ M)	CH4 (μ M)	C1/C2+C3	$\delta^{13}\text{C}_{\text{CH}_4}$ ‰ (VPDB)	$\delta^{13}\text{C}_{\text{CO}_2}$ ‰ (VPDB)	Porosity (%)	Ca (mM)	Mg (mM)
water depth = 1429 m	0.05	29.9	4.1	47.7					80.7	9.8	55.8
Long: 19 01.8100N	1.055	27.5	5.35	66.1	2.0	6.1		-17.9	80.3		
Lat: 85 38.3498E	2.055	26.7	6.45	120.0	3.2				77.5	12.4	66.0
Sea bottom T= 4.6 °C	3.055	25.6	7.9	217.9		4.8			79.2	11.2	66.6
	4.055	24.3	9.35	261.9					77.7	9.8	56.6
	5.055	22.6	12.05	364.7	2.1	7.5			75.1	7.3	58.4
	6.055	20.3	10.45	624.2					74.6	7.2	55.3
	7.055	17.8	10.15	712.4	1.0	9.1			72.8	9.5	55.5
	8.055	16.3	14	749.1	1.5	12.1		-20.0	70.2	6.9	54.3
	9.055	15.1	15.95	749.1					71.7	6.9	59.0
	10.055	13.4	16.4	738.1					74.8	6.0	56.4
	11.55	9.4	19.85	796.8		9.9		-21.6		5.2	50.2
	13.055	7.8	19.55	848.2					75.4	4.8	55.3
	14.55	5.2	21.4	778.5	1.2	6.1	-30.2	-17.4	69.2		
	16.055	2.6	22.9	851.9					67.4	4.6	50.8
	17.55	0.1	25.8	980.4					74.2	3.9	50.1
	19.055	nd	26.15	965.7	284.3	838.6	-99.7	-25.0	69.4	4.8	51.1
	20.55	nd	25.05	987.8	748.7	2102.2			70.2		

22.055	nd	24.45	1156.7						69.8	5.2	62.6
23.55	nd	22.55	1244.8	1659.4	2101.5	-99.2	-18.4		68.4	3.2	46.5
25.055	nd	20.3	1299.9						73.4	4.5	66.5
26.55	nd	21.05	1332.9						69.6	3.1	47.6
28.055	nd	24.05	1395.3	2114.1	924.3	-96.4	-23.0		77.6	4.0	55.9
29.55	nd	22.4	1358.6						70.0	4.0	48.0
31.055	nd	20.5	1725.8	2905.5	2258.5				66.8	4.2	52.6
32.55	nd	22.3	1891.1	8027.7	5138.0	-93.5	-23.1		70.1	4.5	58.4
34.055	nd	21.35	1931.5						76.2	3.4	56.2
35.55	nd	19.15	1865.4		884.4	-92.3	-20.7		73.0	3.3	45.4
37.055	nd	18.75	2056.3						62.4	2.7	44.2
38.55	nd	19.8	2012.2	1714.6	1325.2				65.6	4.5	56.2

MD161-27	Depth (mbsf)	SO4 (mM)	Alk (mM)	NH4 (µM)	CH4 (µM)	C1/C2+C3	δ ¹³ C _{CH4} ‰ (VPDB)	δ ¹³ C _{CO2} ‰ (VPDB)	Porosity (%)	Ca (mM)	Mg (mM)
water depth =1691 m											
Lat:18 57.3707N	0.05	26.5	4.7	91.8	3.9	11.2			81.0	12.4	65
Long: 85 43.4481E	1.055	22.8	4.8	187.3	5.1	12.1	-18.8	-19.4	81.7	9.5	61.3
Sea bottom T= 3.5 °C	2.055	21.9	9.7	323.1					77.1	10.1	61.1
	3.055	18.2	11.05	389.2	2.4	11.7			73.3	9.4	60.5
	4.055	19.7	10.6	459.0					75.9		
	5.055	16.9	11.9	525.1	1.5	12.8		-25.4	71.7		
	6.055	17.1	12.75	448.0					73.6	9.2	57.2
	7.055	16.1	14.35	539.8					73.4		
	8.055	11.6	16.5	686.7	4.7	9.5		-27.9	69.3		
	9.055	10.8	17.65	683.0						8.1	64.1
	10.055	7.3	20.25	727.1	2.0	15.4			69.4	8.8	67.9
	11.55	6.4	23.35	763.8	2.1	18.8	-69.9	-30.7	68.1		
	13.055	3.9	26.45	907.0		772.7			75.3	5.9	56.9

14.55	1.5	27.2	929.0	745.7		-105.0	-28.5	72.9	5.1	49.5
16.055	0.1	25.6	1064.9					70.4	5.7	51.4
17.55	nd	27.45	1149.3					73.2	5.2	58.7
19.055	nd	26.55	1149.3	2976.0	1362.2	-99.4	-22.9	78.1	5.7	59.9
20.55	nd	24.4	1167.7					67.4	8.7	58.0
22.055	nd	23.5	1200.7					67.6		
23.55	nd	21.8	1310.9	2812.2	1166.7	-96.0	-22.2	73.7		
25.055	nd	18.8	1358.6	2146.7	1266.7			67.4		
26.55	nd	18.85	1402.7					68.6		
28.055	nd	20.15		2551.7	1453.6	-94.2	-17.8	69.8		
29.55	nd	18.9	1454.1					70.4		
31.055	nd	20.05		2054.3	932.8	-91.9	-17.7	68.6		
32.55	nd	19.9	1417.4					65.9		
34.055	nd	20.25	1424.7					62.8		
35.55	nd	20.2	1490.8	693.9	578.7	-90.4	-18.0	64.5		

Table-2. Total organic carbon concentration.

	MD161-19		MD161-25		MD161-27
Depth (mbsf)	TOC(wt %)	Depth mbsf)	TOC(wt %)	Depth mbsf)	TOC(wt %)
0.05	1.1	0.05	0.8	0.05	0.9
0.48	1.2	1.055	0.9	1.055	1.2
0.78	1.3	2.055	0.9	2.055	0.7
1.38	1.2	3.055	0.9	3.055	0.9
1.98	1.2	4.055	0.9	4.055	1.0
2.73	1.1	5.055	0.7	5.055	1.0
3.23	1.0	6.055	1.0	6.055	1.2
3.38	1.0	7.055	1.1	7.055	1.0
3.93	1.1	8.055	1.1	8.055	0.9
4.63	1.5	9.055	1.3	9.055	1.1
4.83	1.3	10.055	1.3	10.055	0.7
5.38	1.2	11.555	1.1	11.555	0.7
5.53	1.5	13.055	1.2	13.055	0.8
5.88	1.8	14.555	0.9	14.555	0.9
6.43	1.9	16.055	0.8	16.055	0.9
6.98	1.6	17.555	0.9	17.555	0.9
7.33	1.4	19.055	0.9	19.055	0.8
7.53	2.0	20.555	0.8	20.555	0.7
7.98	1.7	22.055	0.7	22.055	0.7
9.23	1.1	23.555	0.8	23.555	0.7
9.53	1.0	25.055	1.0	23.555	0.6
9.93	1.3	26.555	0.7	25.055	0.7
10.68	1.2	28.055	1.1	26.555	0.9
10.88	1.3	29.555	1.0	28.055	0.9
11.28	1.4	31.055	1.0	29.555	0.8
11.93	1.3	32.555	0.8	31.055	0.8
12.03	1.2	34.055	0.9	32.555	0.7
12.68	1.3	35.555	1.0	34.055	0.6
13.28	1.3	37.055	0.8	35.555	0.7
13.88	1.6	38.555	0.8		
14.48	1.3				
15.03	1.3				
15.18	1.2				
15.78	1.0				
16.13	1.1				
16.58	1.1				
17.23	1.0				
17.73	1.0				
17.88	1.0				
18.53	1.1				
18.68	1.0				
19.13	0.9				
19.88	1.5				

20.33	1.3
20.48	1.4
21.18	1.4
21.68	1.2
21.98	1.3
22.33	1.1
22.53	1.3
22.68	1.4
23.13	1.2
23.48	0.9
23.73	1.0
24.48	0.9
25.13	1.3
25.83	1.1
26.48	1.1
27.18	1.0
27.73	0.9
28.48	1.0
29.13	1.6
29.73	1.1
30.38	0.7
31.13	1.1
31.73	0.9
32.38	1.6
32.73	1.6
33.08	1.4
33.23	1.7
33.53	1.6
33.73	1.7
33.93	1.2
34.38	1.1
35.08	1.5
35.73	1.6
35.88	1.7
36.43	1.3
36.83	1.0
36.98	1.1
37.38	1.3
37.73	1.2
37.98	1.2
38.28	1.2
38.88	1.2
